TALLINN UNIVERSITY OF TECHNOLOGY
SCHOOL OF ENGINEERING
Department of Electrical Power Engineering and Mechatronics

DEEP LEARNING FOR MATERIAL AND OBJECT IDENTIFICATION USING HYPERSPECTRAL IMAGING

SÜVAÕPPE ALGORITMID MATERJALIDE JA OBJEKTIDE KLASSIFITSEERIMISEKS HÜPERSPEKTRAAL-PILDITEHNIKA ABIL

MASTER THESIS

Student: Ali Zahavi

Student code: 177187MAHM

Supervisor: Professor Mart Tamre

Co-supervisor Engineer Dhanushka Chamara Liyanage

Tallinn 2020

AUTHOR'S DECLARATION

Hereby I declare, that I have written this thesis independently.
No academic degree has been applied for based on this material. All works, major viewpoints and data of the other authors used in this thesis have been referenced.

"....." ..... 20…..

Author: .....
/signature /

Thesis is in accordance with terms and requirements

"....." ..... 20….

Supervisor: ….....
/signature/

Accepted for defence

"....."..... 20… .

Chairman of theses defence commission: .....
/name and signature/

Department of Electrical Power Engineering and Mechatronics

THESIS TASK

Student: Ali Zahavi, 177187MAHM

Study programme,
main speciality: MAHM, Mechatronics
Supervisor(s): Professor Mart Tamre, +372 620 3202
Co-supervisor: Engineer Dhanushka Chamara Liyanage, +372 620 3306

Thesis topic:
(in English) INCORPORATING DEEP LEARNING FOR MATERIAL CLASSIFICATION AND OBJECT RECOGNITION USING HYPERSPECTRAL IMAGING
(in Estonian) SÜVAÕPPE ALGORITMIDE RAKENDAMINE MATERJALIDE JA OBJEKTIDE KLASSIFITSEERIMISEKS HÜPERSPEKTRAAL-PILDITEHNIKA ABIL

Thesis main objectives:

1. Influence of illumination sources on hyperspectral imaging
2. Material classification using hyperspectral imaging
3. Object recognition using hyperspectral mobile camera

Thesis tasks and time schedule:

No	Task description	Deadline
1.		
2.		
3.		

Language: English **Deadline for submission of thesis:** "....."....201....a

Student: .... "....."....201....a
/signature/
Supervisor: .... "....."....201....a
/signature/
Consultant: .... "....."....201....a
/signature/
Head of study programme: .... "....."....201.a
/signature/

TABLE OF CONTENTS

TABLE OF FIGURES

TABLE OF TABLES

PREFACE

The thesis topic was provided by the Department of Electrical and Power Engineering and Mechatronics of Tallinn University of Technology.

I am deeply grateful to my supervisor, Professor Mart Tamre, Head of Mechatronics and Autonomous Systems Centre of Tallinn University of Technology, who throughout my studies at Tallinn University of Technology, helped me to find all answers to my questions. Under his guidance, I was able to successfully complete the task and gain a lot of new knowledge.

I would like to thank my co-supervisor, Dhanushka Chamara Liyanage, PhD student of Mechatronics and Autonomous Systems Centre of Tallinn University of Technology, for cooperating with me in writing a thesis-related research paper, and his help in difficulties throughout my studies in Tallinn University of Technology.

Finally, I would like to thank Andrei Palshin, with whom we worked on the thesis-related research paper with the title of "Influence of Illumination Sources on Hyperspectral Imaging" ,and successfully presented it at International Conference on Research and Education in Mechatronics, REM 2019 [1].

LIST OF ABBREVIATIONS AND SYMBOLS

VIS	Visible Spectrum
FWHM	Full Width at Half Maximum
HSI	Hyperspectral Image/ Imaging
BIP	Band Interleaved by Pixel
BIL	Band Interleaved by Line
BSQ	Band Sequential
AVIRIS	Airborne Visible/Infrared Imaging Spectrometer
MLC	Maximum Likelihood Classifier
SVM	Support Vector Machine
NIR	Near-Infrared Spectrum
AI	Artificial Intelligence
CNN	Convolutional Neural Network
LED	Light-Emitting Diode
ROI	Region of Interest
SAM	Spectral Angle Mapper
NN	Neural Network
RGB	Red, Green, Blue (colour model)

INTRODUCTION

General overview

Hyperspectral Imaging (HSI), similar to other spectral imaging, processes the information from the electromagnetic spectrum in order to find or identify different materials or objects by obtaining the spectrum of each pixel in the image of a scene [1]–[3]. On other words, HSI combines the power of spectroscopy and digital image processing in order to classify materials presented in a scene, based on the spectral signatures of each pixel of the image. While HSI is a fast-growing area in the remote sensing field for earth observation; emerging mobile hyperspectral cameras made it possible to use them for material classification and object recognition in the real-world scale.

Furthermore, these days, deep learning achieves recognition accuracy at higher levels than ever before, and recent advances in deep learning have improved to the point where deep learning outperforms humans in some tasks like classifying objects in images [4].

Therefore, to benefit simultaneously from these two powerful technologies (HSI and deep learning) in the real-world scale, this thesis aims to address three major problems related to the deployment of HSI and deep learning for material classification and object recognition.

Problem statement

In this thesis, the effort is to focus on three main problems related to the use of Hyperspectral Imaging (HSI). These problems are as follows:

1. Influence of illumination sources on HSI and finding the most suitable lighting option: Similar to typical machine vision applications, illumination source plays a vital role in acquiring a proper result in HSI. Therefore, it is important to have an understanding of the influence of the illumination source on the output of the imaging procedure. As a consequence, this problem is faced as the first major challenge in this thesis.

2. Material classification using a hyperspectral mobile camera: One of the essential applications of HSI is in the field of material classification, and this gives rise to the importance of providing a generalized suitable method for such classification. As a

result, providing a generalized method to solve this problem is investigated as the second challenge throughout this thesis.

3. Object recognition using a hyperspectral mobile camera: While material classification is counted as the primary capability of HSI, emerging of mobile hyperspectral cameras made it possible to benefit from HSI for the purposes of object recognition in the real-world scales as well. One idea is to solve the problem of recognition by extracting a false RGB image from the HSI, and pass it to a well-known classification algorithm. Considering this idea, one of the initial questions which seems crucial to answer is whether different reconstructed false RGB images affect the accuracy of the classification.

Thesis structure

This thesis is organized in four main chapters, and followed by a summary, references and appendices, at the end.

Chapter 1 presents the literature overview/analysis, which consists of three main sections as hyperspectral imaging, material classification, and object recognition. In this chapter, firstly, it is tried to give an overview of hyperspectral imaging. Then, previous works about material classification using hyperspectral imaging are studied. Next, recent advances in object recognition are presented. Finally, this chapter is finished with a clearer problem statement and the scope of this research as a conclusion.

Chapter 2 provides research and comparison between different illumination sources and their influences on the results of HSI. Also, in this chapter, several spectral signatures of different materials by practical experiments were provided. This chapter is finished with a conclusion about the most suitable illumination source for HSI.

Chapter 3 proposed a generalized method of using mobile hyperspectral cameras for material classification. This chapter compares different classifiers and their required steps. This chapter is finished by introducing the best classifier result according to the scope of this research as the conclusion.

Chapter 4 discusses the idea of reconstructing a false RGB image from an HSI for object recognition. This chapter tries to find the influence of band selection models (different false RGB images) on the performance of a well-known object recognition convolutional neural network. This chapter is finished with a conclusion that answers whether, or not, the model of band selection affects the performance of the recognition agent.

1. LITERATURE OVERVIEW/ANALYSIS

In this chapter, an overview of the theoretical basis, and previous works of hyperspectral imaging, material classification, and object recognition have been presented.

1.1 Hyperspectral imaging

To use Hyperspectral Imaging Technology, knowing the theory behind it, is a must. Therefore, in this section, some fundamentals about spectroscopy and electromagnetic spectrum have been discussed. Also, in the section of terminology, some words such as spectral range, spectral resolution, spatial resolution and spectral signature are briefly explained.

1.1.1 Spectroscopy

In the 16th century, Sir Isaac Newton discovered the dispersion of the light after passing the light through a prism. He observed the light splitting into the colours after passing through a prism, and described the concepts of the first spectrometer [5].

Spectroscopic methods can provide the fingerprints of the materials under experiments using the interaction between the electromagnetic radiation and the sample. Indeed, these interactions can be observed as the amount of energy emitted to the sample by illumination source within a given wavelength range, which has been either emitted or absorbed. Also, the reflected amount of energy from the sample can be calculated [6].

The sample under experiment will absorb, reflect or refract the energy emitted by illumination source depends on the frequency of the light (Figure 1.1). Therefore, this complicated relationship between the frequency of the light and the intensity of absorption can be interpreted as the fingerprint of the sample.

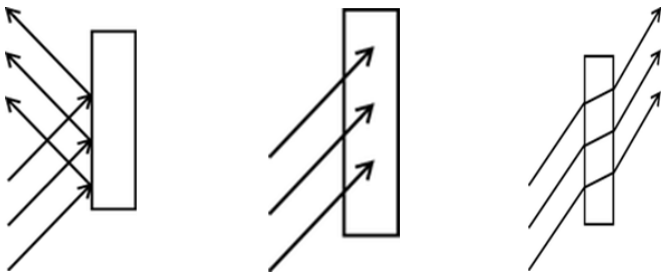

Figure 1.1 From left to right: reflection, absorption and refraction [7]

1.1.2 Electromagnetic spectrum

The word, electromagnetic spectrum, has been used to describe the entire range of light that exists in terms of frequency, wavelength or energy with units of Hertz, meters and electron volts, respectively [8], [9]. It consists of several regions from gamma rays to radio waves (Figure 1.2). Although sometimes these regions overlap, it is more convenient to divide the electromagnetic spectrum. As it is shown in Figure 1.2, an extremely small range of wavelength, between 400 to 700 nm, is visible to human, which has been called *Visible Spectrum (VIS)*.

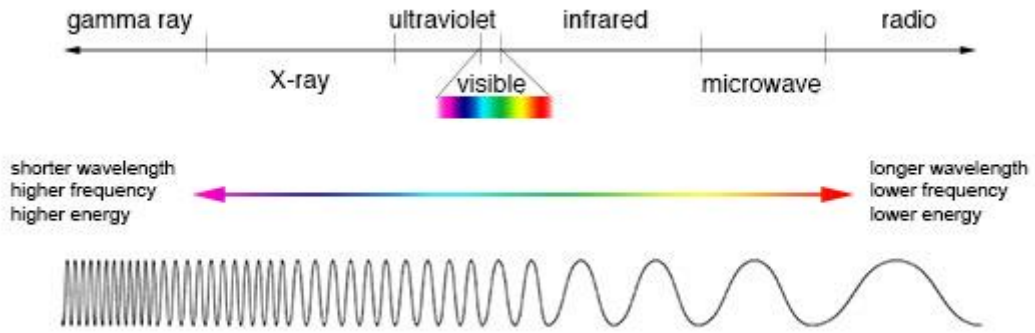

Figure 1.2 Electromagnetic spectrum [5]

1.1.3 Terminology

In Appendix 1, some essential terminologies which generally are used in hyperspectral imaging have been briefly discussed.

1.1.4 Hyperspectral data cube

A hyperspectral image consists of several grayscale images (equal to the number of the bands in the hyperspectral camera). This image represents the reflectance of a pixel at different wavelengths and carries the spatial information in two dimensions (m rows and n columns), as well as spectral information (of k wavelength) [10][11].

A hyperspectral data cube is the term which sometimes used instead of hyperspectral image. This type of image captures a scene in three dimensions ($m \times n \times k$), and for any image pixel, a spectral reflectance graph will be provided [12] (Figure 1.3). In other words, in the hyperspectral data cube, the spectral signature of each image pixel will be presented.

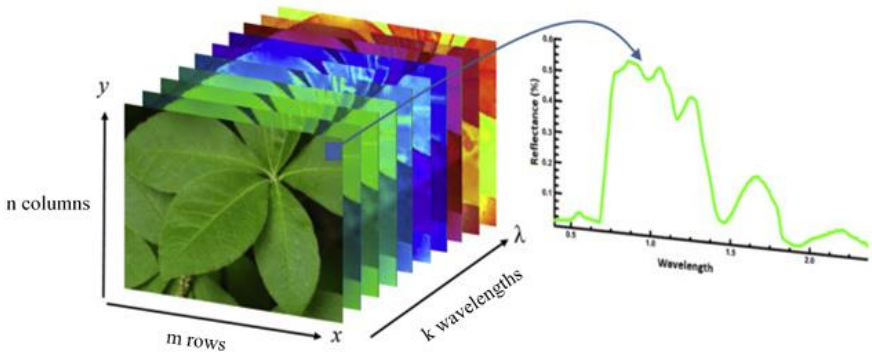

Figure 1.3 Hyperspectral data cube (left), spectral signature of a pixel (right) [13]

1.1.5 Hyperspectral image acquisition

A hyperspectral imaging acquisition system consists of hardware and software parts. There are some standard components in HSI, although the configuration may be different depending on the sample under experiments and the purpose of the acquisition [14]. The main components of an HSI system are the sample, illumination source, hyperspectral camera, objective table and a computer. In Figure 1.4, one example of a configuration of the hyperspectral imaging system can be found.

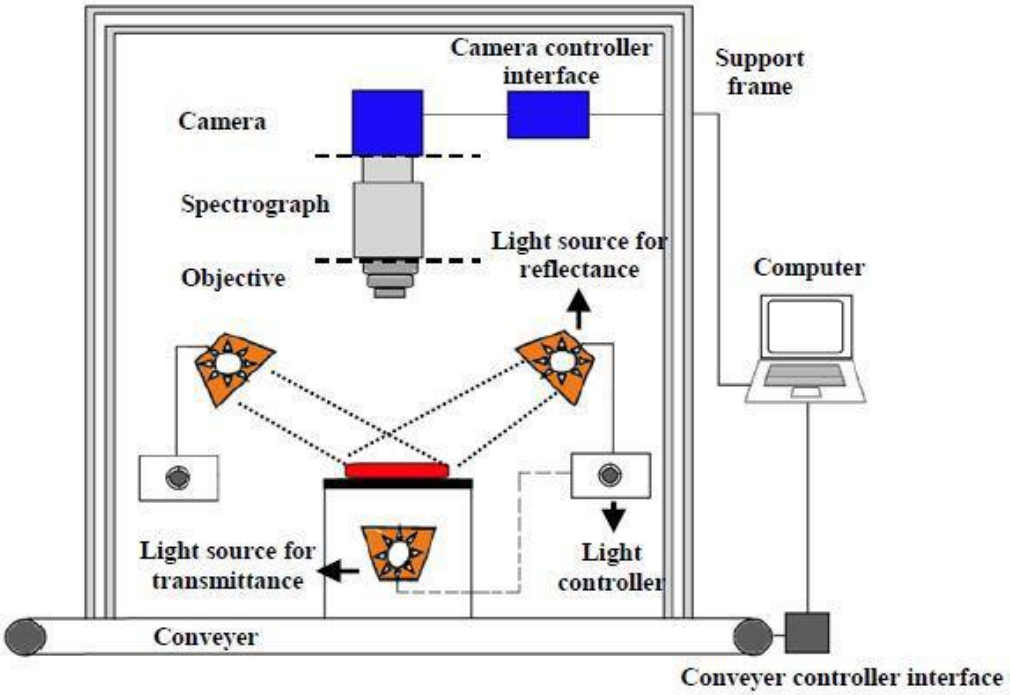

Figure 1.4 Hyperspectral imaging system configuration [14]

There are three main ways to build a hyperspectral cube: point scanning, line scanning and area scanning known as Whiskbroom, Pushbroom, and Tunable filter, respectively [15].

Whiskbroom (point-scan imaging)

Whiskbroom method, also known as point scanning method, builds a hyperspectral image by measuring the spectrum of a single point, and then the sample will be moved, and the next spectrum will be taken (Figure 1.5) [16],[17]. Using this configuration, the hypercube data will be stored as Band Interleaved by Pixel (BIP). The way to write a BIP format is shown in Figure 1.5[18].

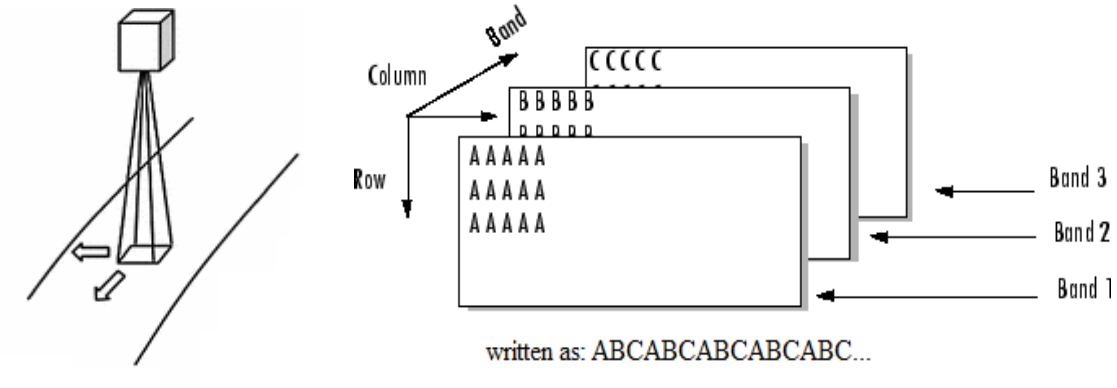

Figure 1.5 Whiskbroom method (left), BIP multiband writing (right) [18]

Pushbroom (line-scan imaging)

Pushbroom method, also known as line scanning method, obtains a part of spectral information of a line of the sample, which will be recorded by an array detector simultaneously (Figure 1.6) [19]. With moving the sensor or the object, the spectral information of that line will be completed. Using this configuration, the hypercube data will be stored as Band Interleaved by Line (BIL) format. The way to write a BIL format is shown in Figure 1.6 [18].

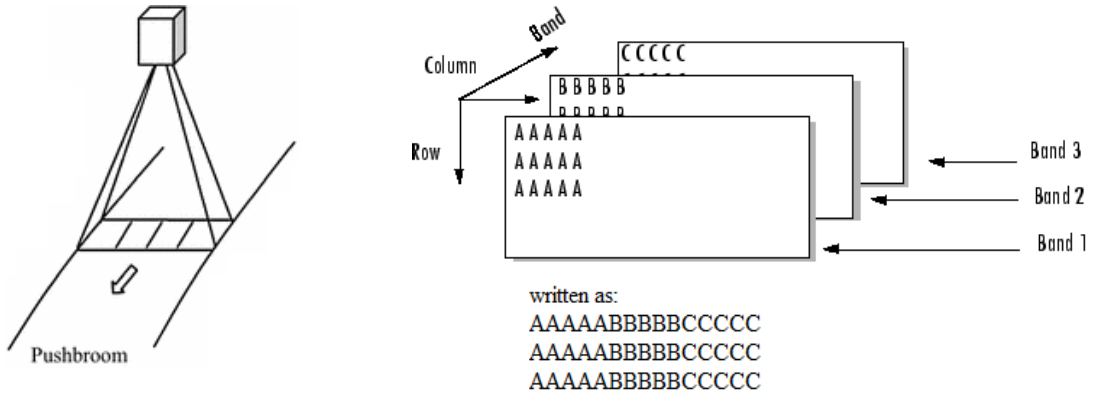

Figure 1.6 Pushbroom method (left), BIL multiband writing (right) [18]

Tunable filter (area-scan imaging)

Tunable filter method, also known as area scanning method, Keeps the image field of view (FOV) fixed, and captures the images one wavelength after another. Therefore, this method called as wavelength scanning or band sequential method as well [20]. Using this configuration, the hypercube data will be stored as Band Sequential (BSQ) format. The way to write a BSQ format is shown in Figure 1.7[18].

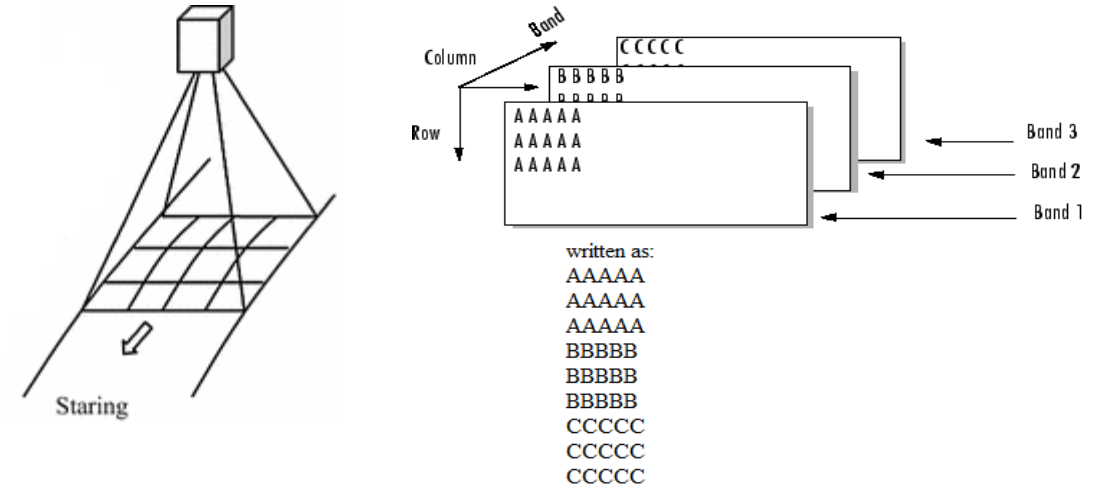

Figure 1.7 Tunable filter method (left), BSQ multiband writing (right) [18]

1.2 Material classification

In this section, previous works about material classification using hyperspectral imaging have been discussed and analyzed.

One of the most important applications of multispectral and hyperspectral imaging is in material classification in remote sensing for the earth observation or land cover in agriculture. The motivation for the development of HSI goes back to 1970' in support of Landsat-1 data analysis. Since the task needed development in both hardware and software, the hardware development was done by NASA/JPL with Airborne Imaging Spectrometer (AIS) in 1983, and in 1987, followed by the one of the best providers of hyperspectral data of this day, Airborne Visible/Infrared Imaging Spectrometer (AVIRIS) [21].

Furthermore, Landsat 8 is the latest version of the Landsat program launched on February 11, 2013, which can provide multispectral data of the earth in 11 bands [23]. The bands and resolutions of Landsat 8 have been presented in Appendix 2.

Land cover classification using Landsat data has been investigated in many researches. One of these researches classified Beijing's land cover. Beijing, the capital of China, is located between latitudes 39°26 and 41°03'N and longitudes 115°25'E and 117°30'E, covering an area of approximately 16,800 km [24]. In this work, Maximum Likelihood Classifier (MLC) and Support Vector Machine (SVM) classified the land into six classes, water, crop, bare land, impervious, grass and forest. Finally, the result of MLC has been compared with SVM (Figure 1.8).

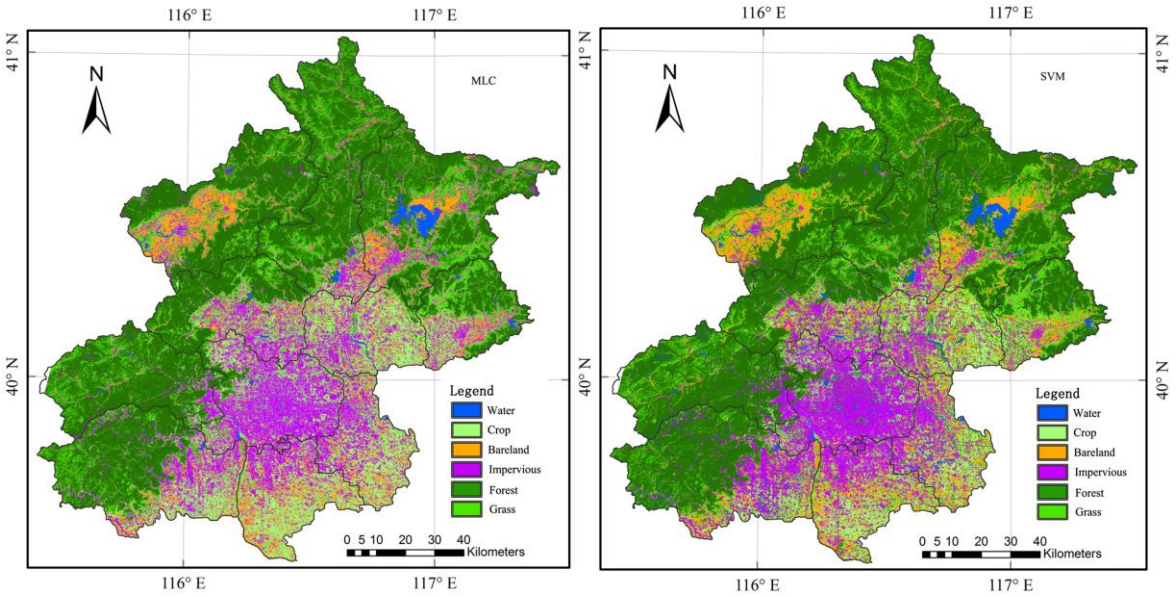

Figure 1.8 Beijing's land cover classification using the MLC (left) and SVM (right) [24]

Another research investigated the comparison of land cover in Eastern Europe using a hybrid classification [25]. In this work, the land cover of Eastern Europe into 10 classes. The classes can be found in Table 1.1. Also, the result of classification has been shown in Figure 1.9.

Table 1.1 Eastern European land cover classes [25]

Class	**Description**
1. Water	Open water, rivers and lakes
2. Dense settlements	Dense built up areas, cities, construction areas
3. Open settlements	Suburbs, villages, small gardens and orchards
4. Broadleaved forest	Minimum fraction of broadleaved trees of 70%
5. Mixed forest	Neither broadleaved nor coniferous species dominate
6. Coniferous forest	Minimum fraction of coniferous trees of 70%
7. Shrubland	Secondary succession on fallow land, early reforestation and heathlands
8. Grassland	Pastures, meadows and unmanaged grasslands
9. Poloniny	High mountain grasslands
10. Arable land	Agricultural areas

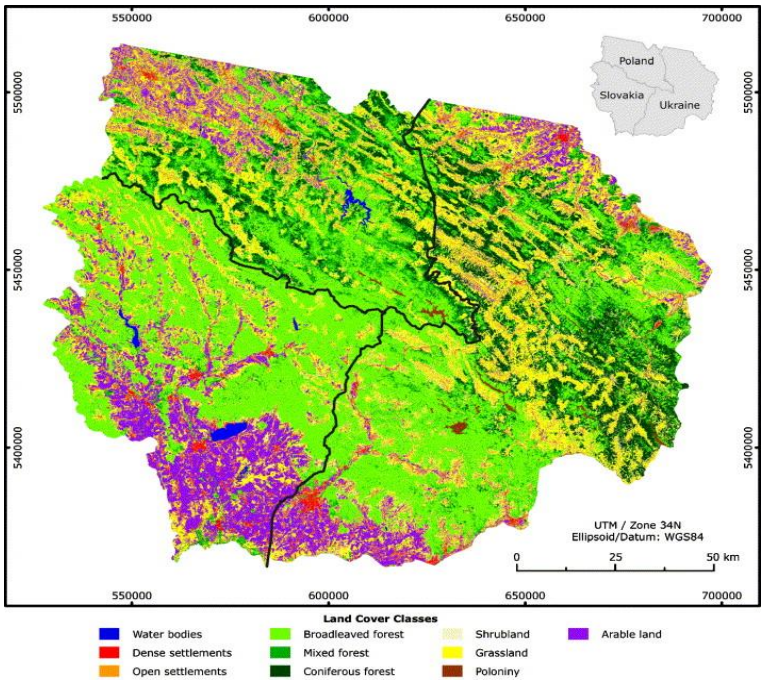

Figure 1.9 Land cover map for the border of Poland, Slovakia, and Ukraine [25]

Another application of HSI can be found in the estimation of material content. For example, in a work that has been published in 2010, estimation of Chlorophyll content of crops using hyperspectral imaging has been investigated, and the reflectance curves of a crop and of bare soil, have been presented (Figure 1.10).

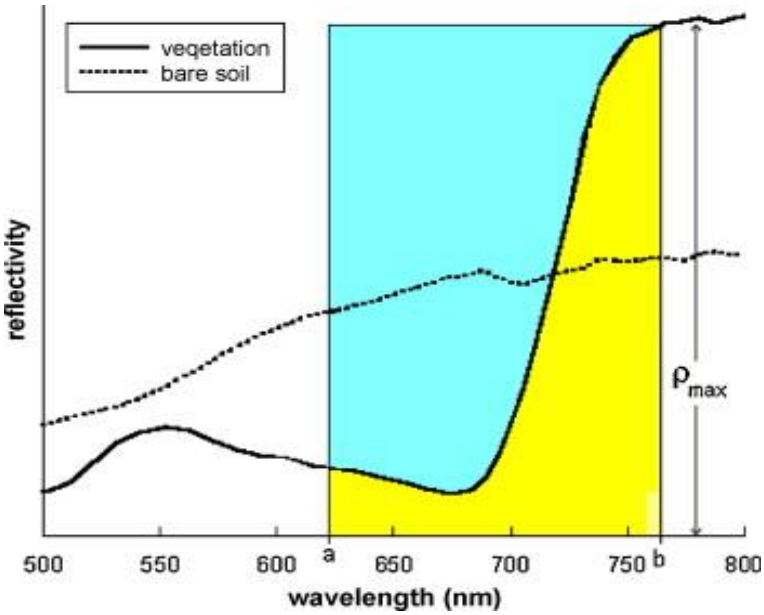

Figure 1.10 Reflectance curves of a crop and bare soil [26]

One of the indoor applications for HSI, which has been investigated in 2008, is human skin detection [27]. The spectral range in this work was between 900nm to 1744nm (NIR). The result has been shown in Figure 1.11.

Figure 1.11 Image of test scene (Top), Skin detection within test scene (Bottom) [27]

1.3 Object recognition

Object recognition may be simply defined as the action of applying semantic attributes to an object, based on observed/captured properties of the object. The method to acquire and select the properties of the object for further process, together with the method to perceive and analyze these properties are vital factors which can make distinctions between different recognition methods. After processing and analysis, the object is assigned an attribute, which in computer recognition, is synonymous to classifying procedure in which the object is assigned to a previously recognized (defined and named) class. Another procedure which can take place during the recognition is the identification of place of the object in the image, or in other words, localizing the object.

Recognition of objects, as stated, can be considered to consist of two sub-level procedures which result in the proper detection of the objects, namely classification and localization. During the classification, the object is analyzed and is assigned a class. Objects in this class should reflect the properties based on which they have been grouped together. Localization takes place when the occupied region by an object in the image is located and identified. The output of localization is some type of indicator of

the place of the object in the image, which is in most cases a bounding box displayed on the image surrounding the object. If the running of the two mentioned procedures shows success, the result will be the detection of the object.

Finally, if there is a need for separation of the object by its occupied region, image segmentation may be done as the last step. Since image segmentation is applied to separate the object, we can call this process object segmentation. Object segmentation is not considered as a critical step in object recognition in its general sense, but segmentation can be of extensive use in applications where the selection of object pixels are of benefit. The outline of the mentioned processes can be observed in Figure 1.12.

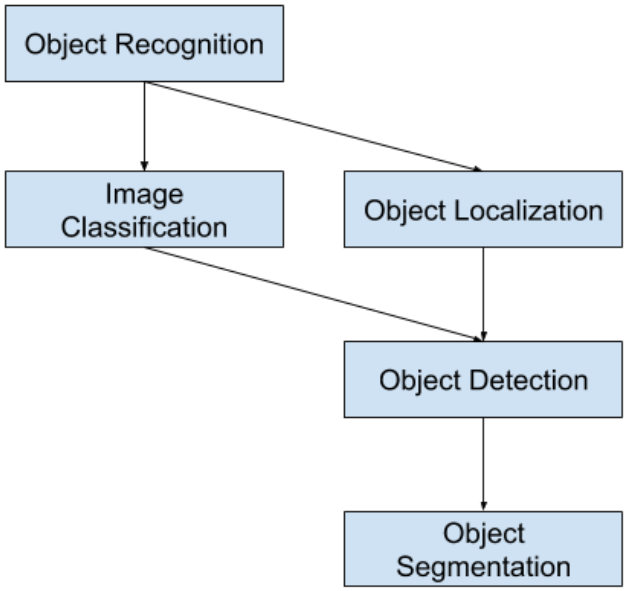

Figure 1.12 The outline of the object recognition process [28]

The result of the process on an image, according to the described mechanism is displayed in Figure 1.13.

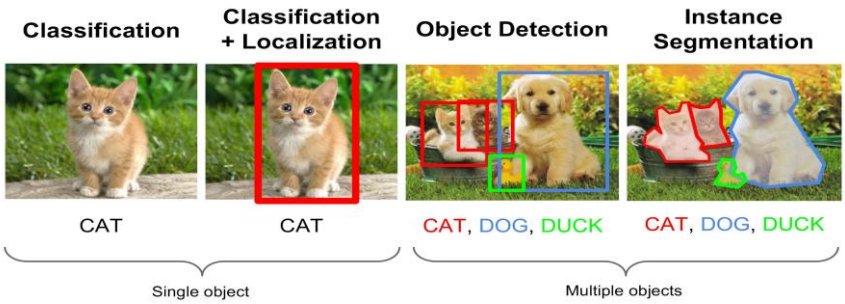

Figure 1.13 The result of object recognition [29]

1.3.1 History of recognition and AI methods

Object recognition has come initially to existence in the scope of concerns of image processing field, and at the start, pure image processing techniques were proposed for the challenges on the topic of recognition. Computer recognition and vision researches have their origins in the early 1960s. One of the earliest applications was pattern recognition systems for character recognition in office automation related tasks [30]. There have been numerous ups and downs in the field since its appearance, but probably the most significant turning point in the recognition has occurred when machine learning paradigms found success during the 2000s and 2010s.

Modern recognition techniques do not solely incorporate image processing algorithms, and deep learning has become a very influencing player in the field in recent years. Deep models can be referred to as neural networks with deep structures. The history of neural networks can date back to 1940s, and the original intention was to simulate the human brain system to solve general learning problems in a principled way. It was popular in the 1980s and 1990s with the proposal of the back-propagation algorithm by Hinton et al. However, due to the overfitting of training, lack of large scale training data, limited computation power and insignificance in performance compared with other machine learning tools, neural networks fell out of fashion in early 2000s. Deep learning has become popular since 2006 and has drastically advanced from that time [31].

1.3.2 Different methods of object recognition

Many methods have been proposed for recognition of the objects since the 1960s. These methods are categorized based on different criteria. In the following paragraphs, some of these criteria are discussed or pointed out.

One classification criterion is based on the approach of the network, and indicates if a network has single-stage architecture or a two-stage architecture. On the one hand, there are two-stage detectors, such as Faster R-CNN or Mask R-CNN, that (i) use a Region Proposal Network to generate regions of interests in the first stage and (ii) send the region proposals down the pipeline for object classification and bounding-box regression. Such models reach the highest accuracy rates, but are typically slower. On the other hand, we have single-stage detectors, such as YOLO (You Only Look Once) and SSD (Single Shot MultiBox Detector), that treat object detection as a simple regression problem by taking an input image and learning the class probabilities and bounding box coordinates. Such models reach lower accuracy rates, but are much faster than two-stage object detectors [32].

Yet another criterion is how many objects in one image can be classified and localized each time the algorithm is applied to the image. Some of the methods make it possible to achieve recognition of multiple objects in a photo, and some of the methods only let for one object to be recognized at once (Figure 1.14).

Figure 1.14 Multiple object recognition (left), one object recognition (right) [33]

YOLO

YOLO (v1) is the first real-time object detectors which can achieve 45fps speed on a Titan X GPU, and its faster version can achieve 155fps (tested on PASCAL VOC 2007) [34]. The core idea behind this fast detector is a single convolutional network consisting of convolutional layers followed by 2 fully connected layers, which simultaneously predicts bounding boxes and class scores [34]. The YOLO model was first published (by Joseph Redmon et al.) in 2015 [35].

A single neural network is applied to the full image. The model works by first splitting the input image into a grid of cells, where each cell is responsible for predicting a bounding box if the centre of a bounding box falls within it. Each grid cell predicts a bounding box involving the x, y coordinate and the width and height and the confidence. A class prediction is also based on each cell. For example, an image may be divided into a 7×7 grid, and each cell in the grid may predict 2 bounding boxes, resulting in 94 proposed bounding box predictions. The class probabilities map and the bounding boxes with confidences are then combined into a final set of bounding boxes and class labels. The image taken from the paper below summarizes the two outputs of the model [28].

When processing is finished for each object, the following information will become available to the network:

- The likelihood that a grid cell contains an object (pobj)
- Which class the object belongs to (c1, c2, ..., cC)

- Four bounding box descriptors to describe the x coordinate, y coordinate, width, and height of a labelled box (tx, ty, tw, th)

Out of these items, only the last two are displayed on the screen in the image area, and the first item is used inside the network. Figure 1.15 shows the workflow of YOLO.

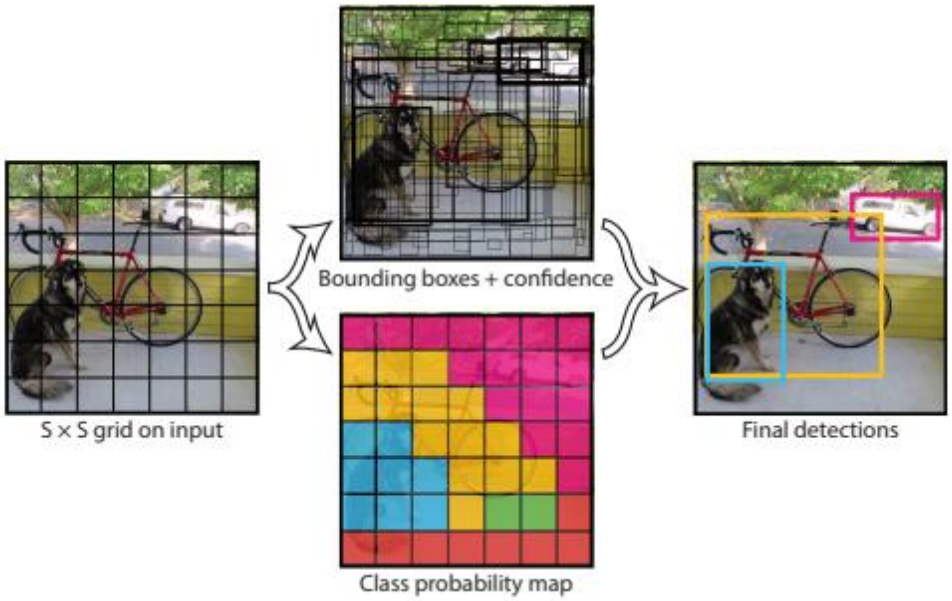

Figure 1.15 YOLO workflow [35]

1.4 Conclusion

In this chapter, it was tried to, firstly, give an overview of the theoretical basis of hyperspectral imaging. Then, previous works of material classification using hyperspectral imaging have been presented. Finally, the object recognition task using deep learning has been explained.

There are three main problems which this thesis tries to address:

1. Influence of illumination sources on hyperspectral imaging: finding the best illumination source for indoor and outdoor hyperspectral imaging applications to acquire a suitable hyperspectral image for further processes is the first problem that this thesis tries to address. There are previous works which have tried to find the influence of illumination sources on different computer vision applications; however, this thesis mostly focuses on this influence on hyperspectral imaging.

2. Material classification using a hyperspectral mobile camera for indoor and outdoor applications: most of the previous works have dealt with using hyperspectral imaging for material classification in remote sensing for earth observation (resolution precision in meters); however, this work focuses on material classification using hyperspectral mobile cameras by acquiring images with higher resolutions (resolution precision in millimeters).

3. Object recognition using a reconstructed false RGB image from a hyperspectral image: since hyperspectral mobile cameras are capable of acquiring the images with the resolution precision in millimeters, they can be used in recognition applications related to objects in real-world scale. Extracting a false RGB image from a hyperspectral image is the initial step for object recognition procedure. The idea of object recognition in real-world scale will help to merge recognition with material classification results for a single hyperspectral image. For this purpose, this thesis tries to investigate the influence of band selection (different extracted false RGB images) on the performance of a well-known pre-trained CNN (YOLO).

2. INFLUENCE OF ILLUMINATION SOURCES ON HSI

This chapter of the thesis, firstly, discusses the influence of different illumination sources on hyperspectral imaging. In order to find the most suitable illumination source for hyperspectral image acquisition, sun, fluorescent, light-emitting diodes (LED) and incandescent light sources have been used. The hyperspectral images were acquired using two hyperspectral cameras, Resonon Pika II in the range of 400-1000 nm and Resonon Near Infrared camera in the range of 1000-1700 nm. Then, the results have been compared with the literature [1].

The second part of this chapter presents the spectral signatures of different materials including Aluminium Oxide (Al2O3), Aluminium Oxide plus Cubic Boron Nitride (cBN), and Wood by using two hyperspectral cameras, Resonon Pika II and Resonon Near Infrared, by the presence of incandescent lights as the illumination source.

2.1 Investigating the influence of illumination source

Like other Machine Vision's applications, illumination source plays a vital role in the validity of extracted data. As a practice, the HSI experiments by the presence of different illumination sources, including sun, fluorescent, LED and incandescent has been done to find the best light source for hyperspectral image acquisition.

2.1.1 Sun

In the literature, the solar spectrum distribution entering the lower part of the atmosphere has been investigated (Figure 2.1). As one can see, the intensity is highest in the light blue region, around 460 nm.

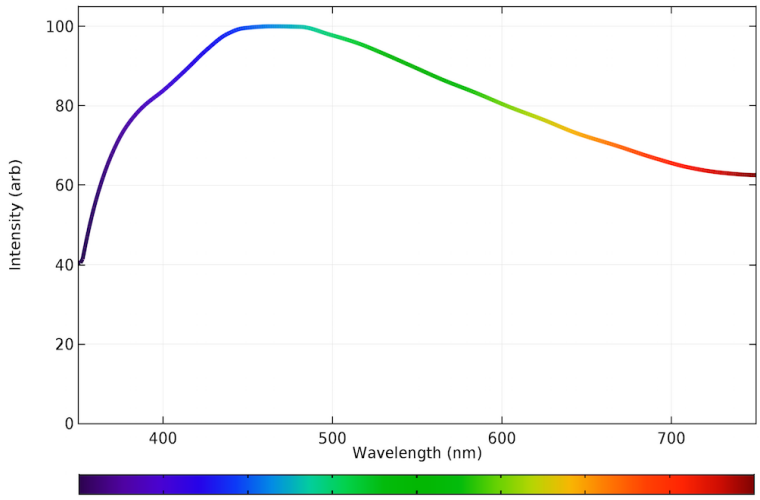

Figure 2.1 Solar spectral distribution entering the lower parts of the atmosphere [36]

In an HSI intensity distribution graph of an object (having some has other peaks or depths), we will be able to state that probably these peaks or depths belong to a material or object absorption. The precise statement needs more experiments with different lighting sources. If the peaks or depths remain in all the graphs for different illumination sources, one certainly can say they belong to the material or object.

The simple spectral distribution of the illumination source will help to distinguish peaks or depths related to the material absorption from the illumination source. From this aspect, the sun seems good for being as a test example of the illumination source. However, many factors may affect the above graph (Figure 2.1) such as geographical location, air pollution, etc.

2.1.2 Fluorescent

A typical fluorescent lamp consists of a low-pressure mixture of mercury and a rare gas like Argon. Following figure (Figure 2.2) shows the Fluorescent lamp spectral distribution. As one can see in the graph, the fluorescent light spectrum is full of peaks and depths. It means this illumination source will emit a different amount of energy in different wavelengths. It is recommended not to use the fluorescent light for hyperspectral image acquisition, because it will be hard to distinguish if peaks or depths belong to this source from the peaks for material absorption. Also, there are two significant peaks for this light source around 540 nm and 620 nm which mean in these two wavelengths, the fluorescent light source emits a large amount of energy to the environment.

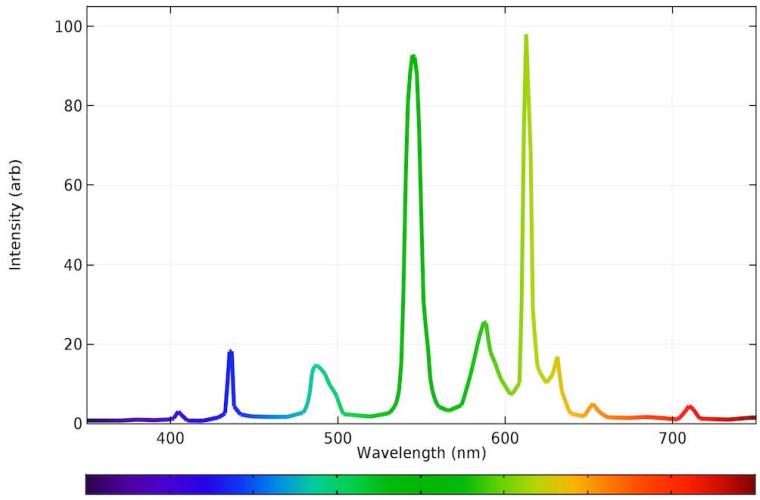

Figure 2.2 Fluorescent spectral distribution [36]

2.1.3 LED

These days, LEDs are known as an efficient illumination source in the industry because they are often more efficient in term of luminous and more durable than traditional incandescent lights [36]. In the following figure, one can find LED light spectral distribution (Figure 2.3). As can be seen in the graph, there is only one peak around 450 nm (Blue), which means this source will emit a large amount of energy in this wavelength. Because unlike incandescent bulbs, LEDs emit light over a narrow range of wavelengths, one can state that LED light seems good enough for the visible range of spectrum and able to distinguish the peaks for the light source from peaks or depths belong to material (object) absorption. However, from the experiments have been done with hyperspectral cameras in the range of 400 nm to 1000 nm, it seems that beyond 750 nm, LED spectrum will have many peaks and depths (recognized as noise). Therefore, it is suggested to use LED light only in the range of 380 nm to 700 nm.

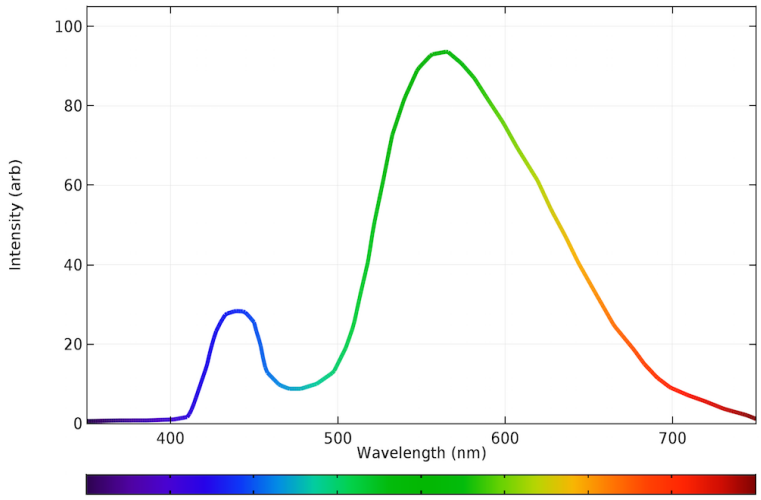

Figure 2.3 LED spectral distribution [36]

2.1.4 Incandescent

An incandescent light bulb has a tungsten filament which is heated when the current is conducted through it. In the following figure (Figure 2.4), one can find the incandescent lamp spectral distribution. Although it is for an ideal incandescent light, one can understand that if some depths during HSI in the visible range have been seen, it can be interpreted as material (object) absorption.

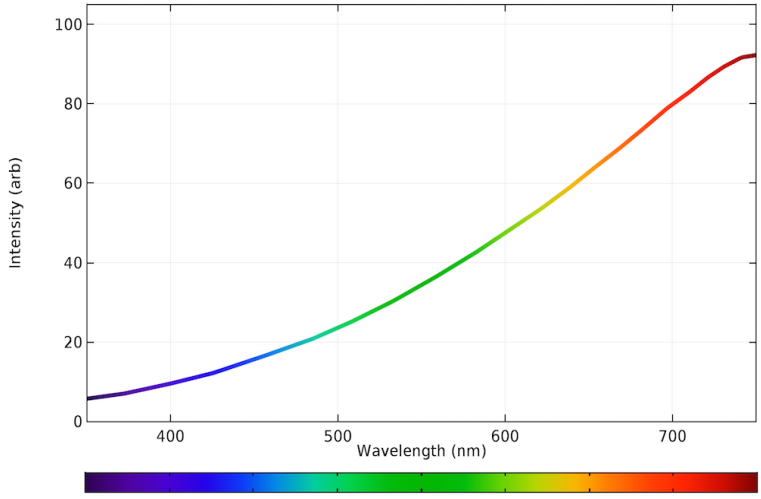

Figure 2.4 Incandescent bulb spectral distribution [36]

2.1.5 The most suitable illumination source

As it is mentioned before in this section of the thesis, simple light source spectral distribution will help to distinguish peaks or depths related to material absorption from

illumination source. From this aspect, all typical light sources except fluorescent seem suitable for different machine vision applications such as HSI in the visible range. Also, LED emits light in a narrow range of wavelength, which causes to be suitable for visible range, not NIR.

Furthermore, as it is discussed, many factors will have an effect on the amount of sun's energy which is entering the lower part of the atmosphere. Therefore, the incandescent light bulb has chosen as the best light source for the different machine vision application such as HSI. In the following table (Table 2.1), one can find the best operational range of each illumination source.

Table 2.1 Comparison of illumination sources

Light sources	380-700nm	400-1000nm
Sun	✓	✓
Incandescent	✓	✓
Fluorescent	×	×
LED	✓	×

2.2 Experiments

This part of the chapter provides the spectral signatures of different materials including Aluminium Oxide (Al_2O_3), Aluminium Oxide plus Cubic Boron Nitride (cBN), and Wood by using two hyperspectral cameras, Resonon Pika II and Resonon Near Infrared, by the presence of incandescent lights as the illumination source.

All the experiments have been performed in a dark room with only the presence of incandescent light as the illumination source without any external light interference. Figure 2.5 shows the test setup. The camera was located directly above the investigated material, and the light sources were located to the left and right of the object, and the material was located on the table covered with light-absorbing material.

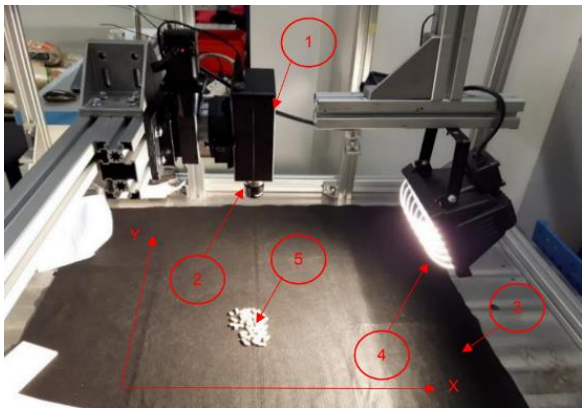

Figure 2.5 test setup, 1. camera 2. optic lens 3. light-absorbing material 4. incandescent light 5. material or object

For each material, a series of images with two hyperspectral cameras (Resonon Pika II, and Resonon Near Infrared) were acquired. The graphs represent the average value of the spectral distribution of the surface of the material. Abbreviation NIR stands for the camera that operating in the near-infrared range (Resonon Near Infrared), and VR for the camera operating in the visible range (Resonon Pika II). Three vertical lines on VR graph is related to RGB colour spectra. The first one is for blue, the second is for green and the last is for red.

2.2.1 Aluminium oxide (Al_2O_3)

In Figure 2.6, taken by NIR, the spectrum of aluminium is almost flat over the entire range. There is no significant peak of aluminium, because they are outside of the NIR camera range [37], [38]; however, it can be seen in Figure 2.6 that using an incandescent lamp causes in minimizing the effect of the light source on the absorption of the material because of the fact that the light source emission spectrum is almost uniform over the entire considered range.

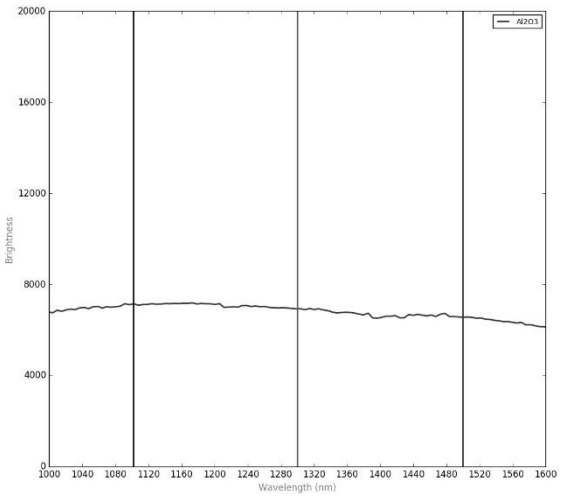

Figure 2.6 NIR image of AL_2O_3

Figure 2.7 shows an image taken by VR camera in the range of 400 – 1000 nm and it is very similar to the incandescent light bulb graph (Figure 2.4) (The brightness increases from 300 nm to 900 nm on the whole interval).

In this experiment, the surface of the material was uneven. For this reason, small fluctuations that slightly affect the intensity of light absorption by the material, have been observed.

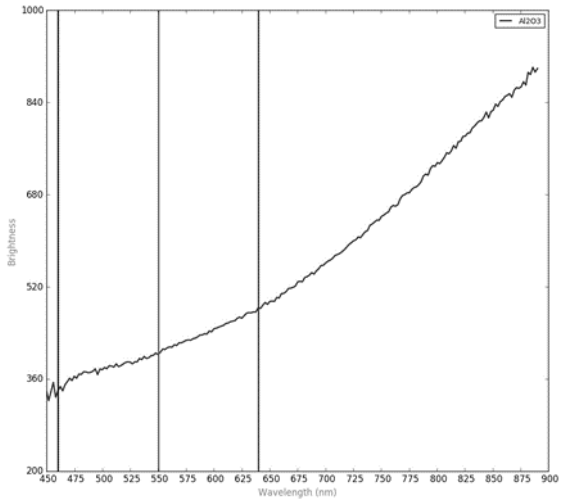

Figure 2.7 VR image of AL_2O_3

2.2.2 Aluminium oxide (Al_2O_3) plus cubic boron nitride (cBN)

To further explore the possibility of identifying the material, aluminium oxide interspersed with a cubic form of boron nitride (cBN) has been tested [39].

Figure 2.8 and Figure 2.9 show the spectral distribution of Al_2O_3 + 10% cBN over the range of 400 nm – 1700nm. There are differences in the amount of light absorption in this experiment and the previous one (pure aluminium) because the position of the material relative to the light source has been changed; however, similar oscillations about 1380 nm could be observed in both experiments.

Furthermore, another test with more cBN interspersed to aluminium oxide (20%), has been done, and it is concluded that increase in the amount of cBN in aluminium oxide did not affect the results, and all in all, the spectrums were almost the same as the pure aluminium oxide spectral distribution in this range of spectrum.

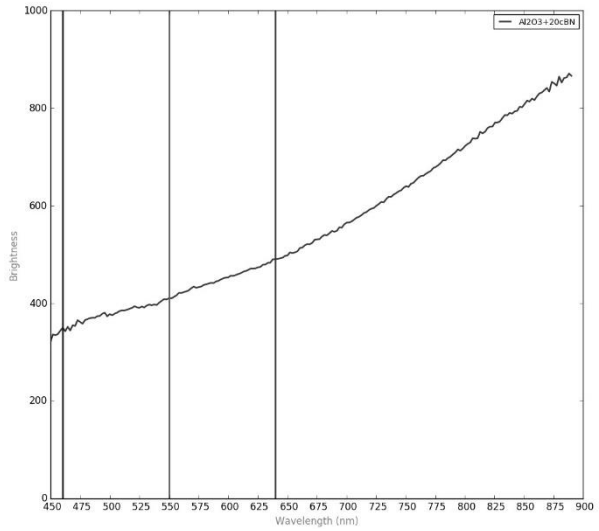

Figure 2.8 VR image of Al_2O_3 + 10% cBN

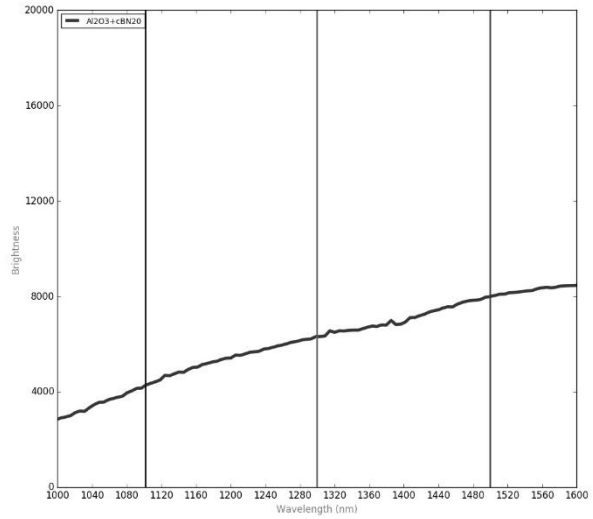

Figure 2.9 NIR image of Al_2O_3 + 10% cBN

Therefore, the absorption spectrum peaks for aluminium oxide with cBN are outside the operating range of our cameras. Also, changes in the composition of the material had no effect on the spectra captured by cameras. However, it can clearly be seen that the incandescent light source does not add any significant peaks to the result, and its influence in any calculations can easily be suppressed.

2.2.3 Wood

The last material taken for the experiments was wooden chips consisting of different types of wood. Figure 2.10 and Figure 2.11 show the spectral distribution of wood chips over the range of 400 nm – 1700nm.

Unlike the previous materials, the peak of the absorption spectrum of wood chips is in the range of the infrared camera (Figure 2.11). Peaks on the chart clearly indicate the presence of water in the tested material [40]; however, Figure 2.10 which contains data about the wood in the visible range shows that there is no data about the material in this range because it is very similar to incandescent bulb spectral distribution.

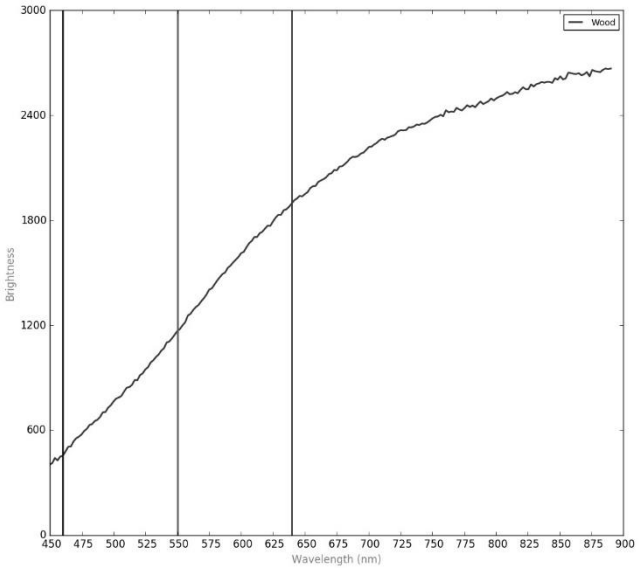

Figure 2.10 VR image of wood

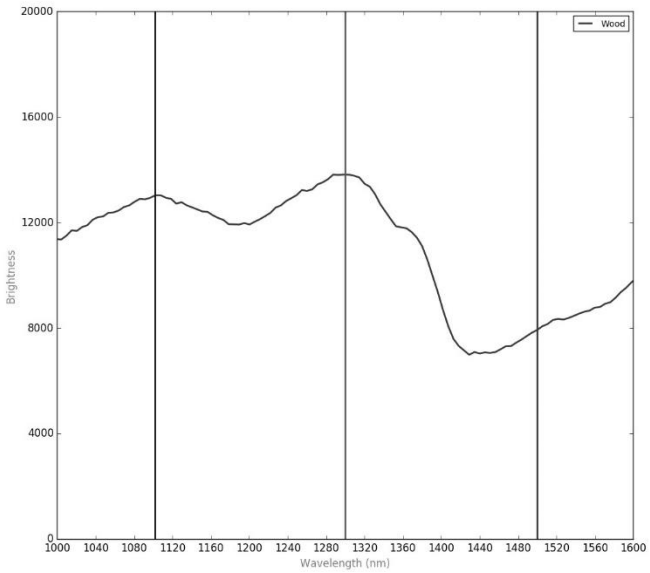

Figure 2.11 NIR image of wood

2.3 Conclusion

Graphs of light absorption of all tested materials show that the use of incandescent lamps for hyperspectral imaging is optimal in terms of covering a wide spectral range of light. Also, this light source adds no significant peaks throughout the operating spectrum. This makes it easy to neutralize its influence in the analysis of the results of hyperspectral imaging and further calculations.

Furthermore, significant peaks belong to water have been observed in the NIR range; however, other tested material did not show any peaks neither in visible range nor near-infrared. In other words, identifying pure aluminium oxide, and aluminium oxide with cBN in the range of 400- 1700 by using hyperspectral imaging was impossible because no peaks or depths belong to these materials have been observed.

3. MATERIAL CLASSIFICATION

In this section, material classification using hyperspectral imaging will be discussed. First, a workflow for solving this task has been presented. Then, the steps have been explained using practical experiments.

3.1 Workflow

As it is presented before in this thesis, the result of hyperspectral image acquisition is a cube (three dimensions: rows, columns and wavelengths). Each pixel in this cube has a spectral distribution over the spectral range of the camera, and this spectral signature should be used to recognize the material belongs to the pixel (Figure 3.1). Therefore, the workflow to solve a material recognition task is the pixel-based classification by meaning of extracting the spectral signature of each image's pixel one after another, and then, solving a classification problem by using their spectral signature.

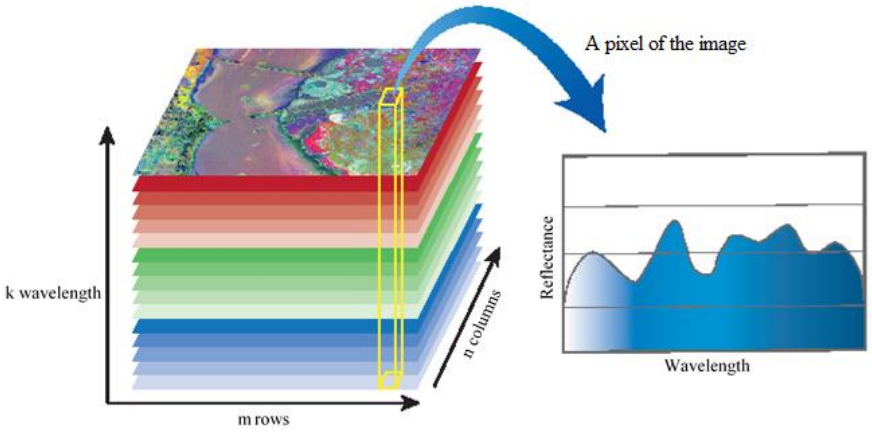

Figure 3.1 Pixel-wise observation of an HSI cube [41]

3.2 Image acquisition

In this work, both indoor and outdoor experiments for material recognition have been tried, and in this section, the hyperspectral image acquisition consists of a camera, illumination source, structure for indoor application, etc. have been discussed.

3.2.1 Camera

The camera used for both indoor and outdoor applications was SPECIM IQ hyperspectral mobile camera (Figure 3.2). The most important technical specifications of this camera

have been shown in Table 3.1. Also, the list of bands of this camera has been presented in Appendix 3.

Figure 3.2 SPECIM IQ hyperspectral mobile camera [42]

Table 3.1 Technical specifications of SPECIM IQ [43]

Spectral range	400-1000 nm
Number of the bands	204
Spectral resolution FWHM	7 nm
Spatial sampling	512 pix
Acquisition mode	Pushbroom (line-scan imaging)

3.2.2 Illumination source

Regarding the illumination source, as it is discussed before, for indoor applications, a typical incandescent bulb, and for outdoor applications, the natural light (sun) have been used.

3.2.3 Test setup

For indoor applications, a test setup has been assembled to install the camera and incandescent bulb in an appropriate height above FOV (Figure 3.3).

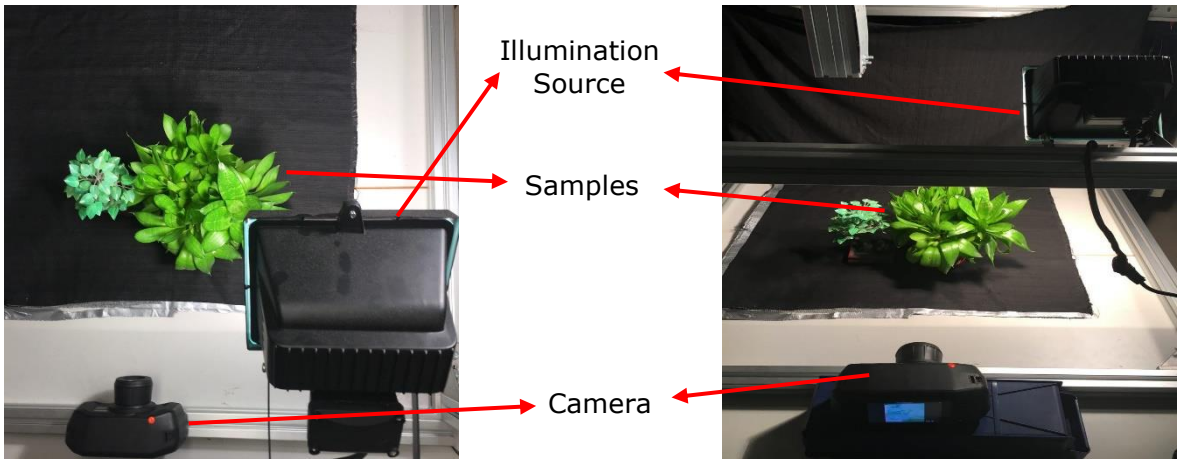

Figure 3.3 Test setup from the top view(left), front view(right)

3.3 Spectral signature of the samples

Figure 3.4 shows a false RGB colour of a hyperspectral image and the selection of a region of interest (ROI) using SPECIM IQ Studio software [44]. This ROI has been chosen to have both real and fake leaves inside for further analysis.

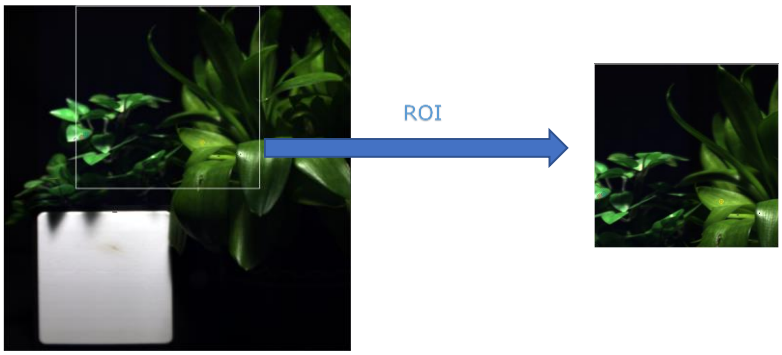

Figure 3.4 Selection of ROI

Spectral signatures of the sample pixels of real and fake leaves have been shown in Figure 3.5. The real and fake leaves have been presented in a single image to determine the capability of HSI for classifying them into two different classes. This test can show whether HSI is capable of distinguishing between two different materials with almost the same color.

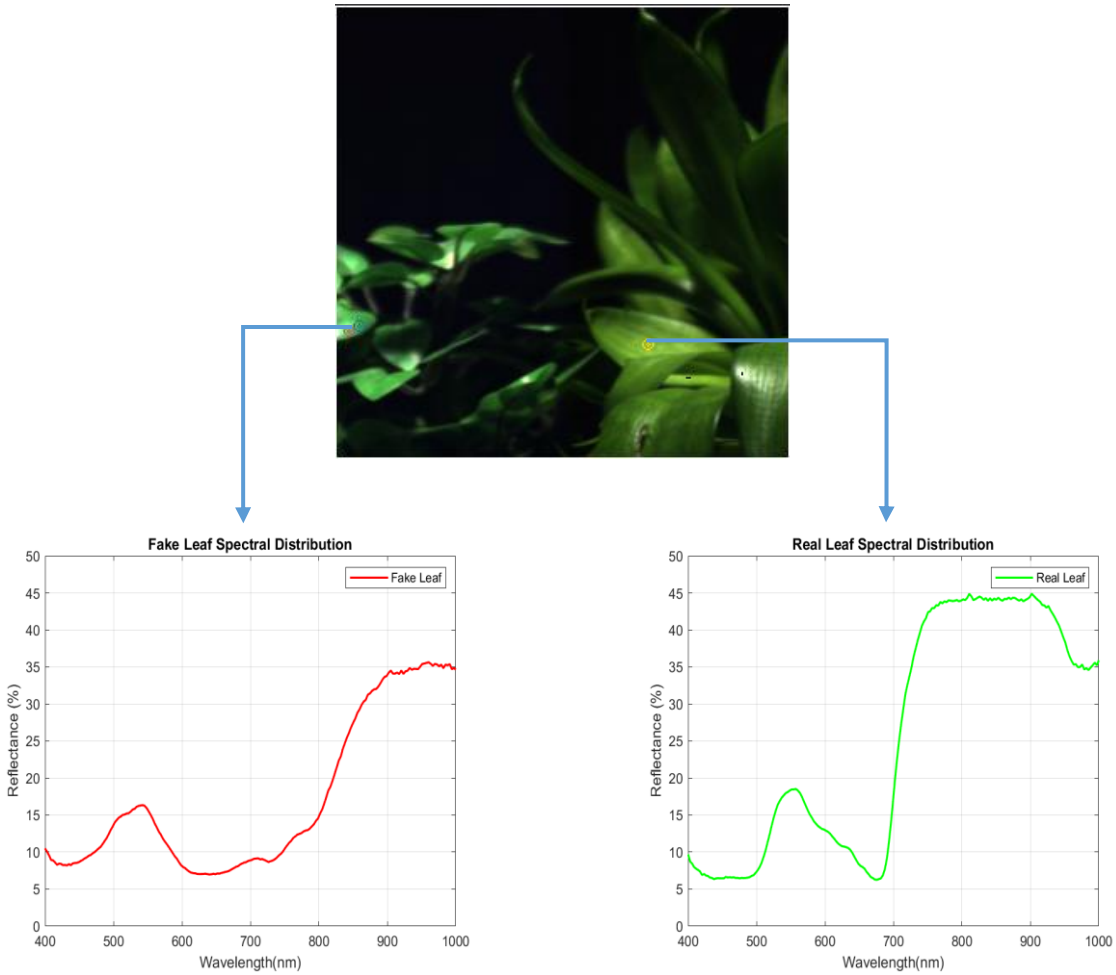

Figure 3.5 The spectral distribution of real and fake leaves

3.3.1 Smoothing the spectral signature (preprocessing)

Generally, measured spectral distribution using a hyperspectral camera carries noises. To remove this noise from the signal, the Savitzky-Golay filter has been used. This filter has been used because it smooths the signal and helps to improve the ability of further processing to identify absorption peaks related to material [45], [46]. Also, applying this filter is fast and simple to implement, in MATLAB (following code). The result, after applying the Savitzky-Golay filter on two selected pixels of real and fake leaves can be seen in Figure 3.6. This filter command in MATLAB is as below:

```
SGolay_Real = sgolayfilt(Real(:,2),3,21);%(Raw real spectral
signature,polynomial order, frame length)
```

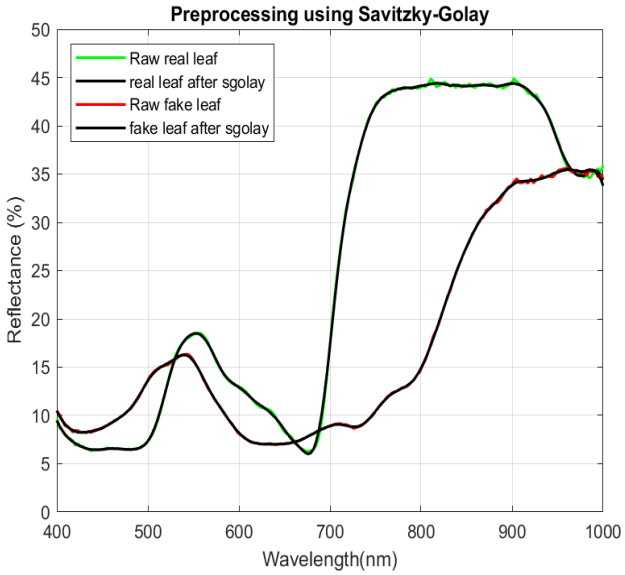

Figure 3.6 Preprocessing (smoothing the spectral signature)

After preprocessing the spectral signatures, these smoothed graphs have been saved as the references for different classes. In the first example of this section, two graphs have been saved separately to show the real and fake leaves classes, and a region of interest (ROI) has been selected. Then, in the next step, the work has been expanded to selecting several classes, not two, and be able to apply to all data cube pixels, not a selected ROI.

There are several classifiers which can be used to solve this material classification task. Indeed, these methods classify the hyperspectral cube, pixel by pixel, based on comparing the spectral signature of that pixel with the references.

In this section, two classifiers have been tested, and the result has been compared. The first classifier, Spectral Angle Mapper (SAM) does not need any prework (feature selection), and it can be applied directly into the hyperspectral cube, although the second classifier, neural network, needs feature selection before classifying the hyperspectral cube.

3.4 Spectral Angle Mapper (SAM)

As it is discussed before, the goal in the material classification using HSI is to distinguish between spectrally similar (but unique) materials [47].

The most critical assumption in Spectral Angle Mapper (SAM) classifier is that a single pixel of the hyperspectral image can be assigned to only one class. The SAM algorithm determines the spectral similarity between two spectra by calculating the angle between

the two spectra, treating them as vectors in a space with dimensionality equal to the number of bands. This angle can be calculated from Equation 3.1 [47]–[49].

$$\alpha = \cos^{-1}\left(\frac{\sum_{i=1}^{NB} a_i b_i}{\sqrt{\sum_{i=1}^{NB} a_i^{\,2}}\sqrt{\sum_{i=1}^{NB} b_i^{\,2}}}\right) \qquad \text{Equation 3.1}$$

Where α is the angle between two spectral graphs, NB is the total number of the bands, a_i and b_i are the reflectance of the reference and sample pixel in i th wavelength of the image.

The equation can be written in MATLAB as below [50]:

```
Alpha = acos(dot(a,b)/ (norm(b) * norm(a)));%Note:a,b are vectors
```

The output of the above command is an angle in radians. If this angle is small enough, it can be interpreted that graphs are spectrally similar to each other. Pixels with greater angles than the specified maximum angle threshold in radians are not classified [48].

Therefore, for distinguishing fake and real leaves example, running SAM for two times (equal to the number of classes) is required. Then, the image should be masked according to the classifier result. The workflow and the result of SAM classifier using SPECIM IQ Studio software [44] can be seen in Figure 3.7.

Furthermore, the code for SAM classifier in MATLAB has been written by the author that allows the user to classify all pixels of data cube, and define different classes. The result of the code for the same example with four different classes (Real-Leaf, Fake-Leaf, White-Reference and Background) has been shown in Figure 3.8.

One note regarding using SAM as the classifier is that depending on the selected spectral signature as the reference of the class, and the maximum angle threshold defined in the program, the result may be different.

The elapsed time for SAM to classify a hyperspectral data cube (512 by 512 by 204) into four classes was around 30 seconds. It means that four each class, the elapsed time was around 6 seconds.

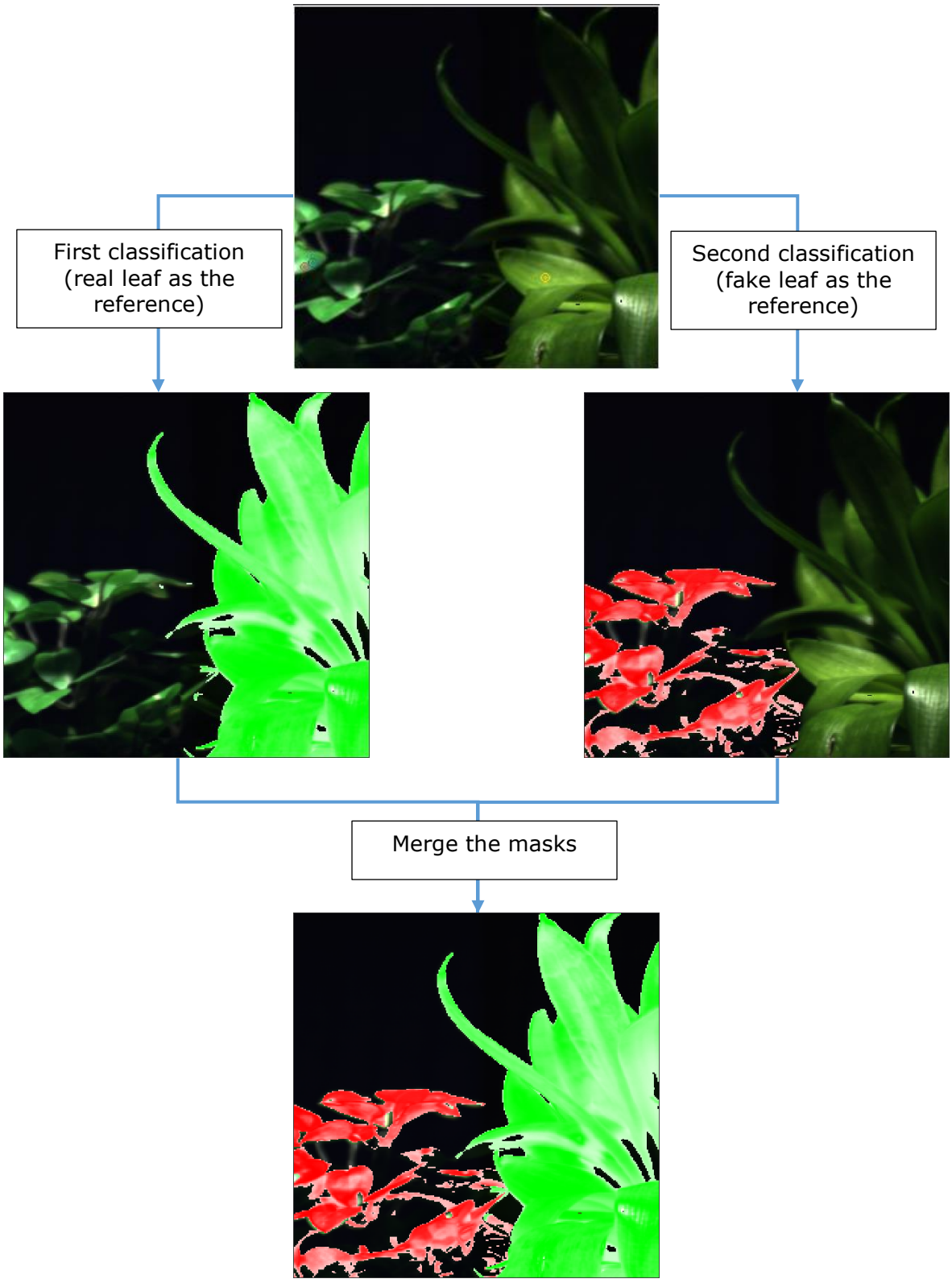

Figure 3.7 SAM classifier workflow and result for fake and real leaves example

Figure 3.8 SAM classifier in MATLAB

To calculate the test performance of this classifier, the original image has been masked manually. Then, the number of pixels which have been classified correctly has been divided by the total number of pixels in the image. The final number shows the accuracy of the classifier (Equation 3.2).

$$\text{Test\_Performance} = \frac{\text{The number of pixels classified correctly}}{\text{The total number of pixels}} \qquad \text{Equation 3.2}$$

The test performance of SAM classifier on this image was 57,81%.

3.5 Neural Network

Despite SAM, neural network (NN) classifier needs feature selection as preprocessing. The reason behind feature selection is that it may take several days or months to run a NN classifier on a hyperspectral cube by dimensions of 512 by 512 by 204 [51]. These dimensions mean 204 features for a pixel for the classification task. Also, the number of inputs in the example (Real-Leaf, Fake-Leaf, White-Reference and Background) that needs to be classified is $512 \times 512 = 262{,}144$. With having 204 features and 262,144 inputs, using NN before feature selection might lead NN to poor result or getting overfitted. Indeed, Feature selection, by identifying the most salient features for learning, focuses a learning algorithm on those aspects of the data most useful for analysis and future prediction [52].

3.5.1 Feature selection

Before running NN classifier, two different methods for feature selection (band selection) have been tested, local extremums of spectral signatures and adding Max-pooling operation.

Local extremums

As it is discussed before, the local extremums of a spectral signature play a crucial role in a material recognitions. Therefore, the code in MATLAB has been written by the author to select the all spectral signatures local minimums and maximums of different references samples. Then, the layer of selected bands have been extracted from the original hyperspectral data cube, and form a new smaller data cube.

In the example of classification of real and fake leaves, 11 wavelengths in total (local extremums of a real leaf, fake leaf and white reference spectral signatures) have been chosen (Figure 3.9) (Table 3.2).

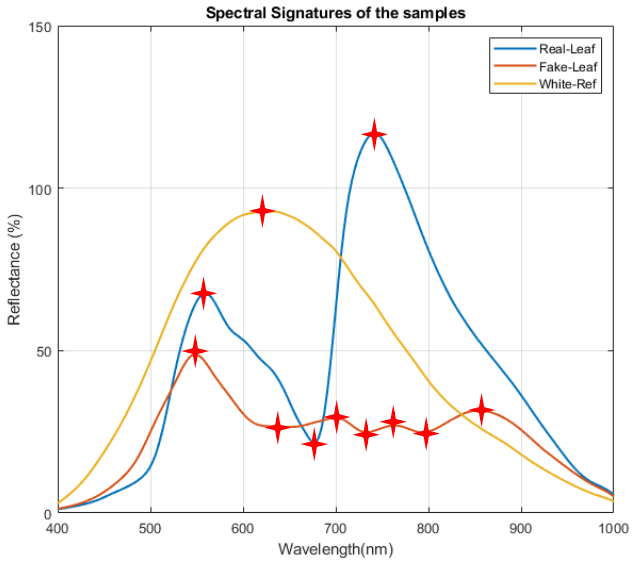

Figure 3.9 local extremums of three spectral signatures

Table 3.2 Selected wavelengths using local extremums

Layer Number	53	57	80	87	96	104	115	118	125	135	155
Wavelength (nm)	548	560	628	648	675	699	732	741	762	792	853

Max-pooling operation

A pooling layer reduces the dimensionality of the input by a constant factor [53]. Generally, its function is to reduce the spatial size for reducing the number of features or parameters needed to be computed in NN [54]. The most common types of pooling operations are max-pooling and average-pooling. The way how these operations work is that they take the maximum / average of the selected region and create a new matrix which each element of the matrix is the maximum / average of the original matrix (Figure 3.10).

In general, the problem of applying maximum / average pooling on a hyperspectral cube is that this layer will be applied to a 2-D matrix, and if this matrix has been considered as the layers of the data cube (k images, where k is equal to the number of the bands), it only helps to reduce the dimensions in spatial size of the hyperspectral image not reducing the number of the bands (as the features of the NN classifier). In other words, it helps to decrease the numbers of inputs, not the features. This problem can be fixed by rotating the hyperspectral cube 90 degrees and applying the maximum / average pooling on the matrix which one of the dimensions shows the wavelengths bands (λ). In Figure 3.11, the grey surface shows the layer that pooling operation is applied to it for general computer vision application and its difference in case of HSI.

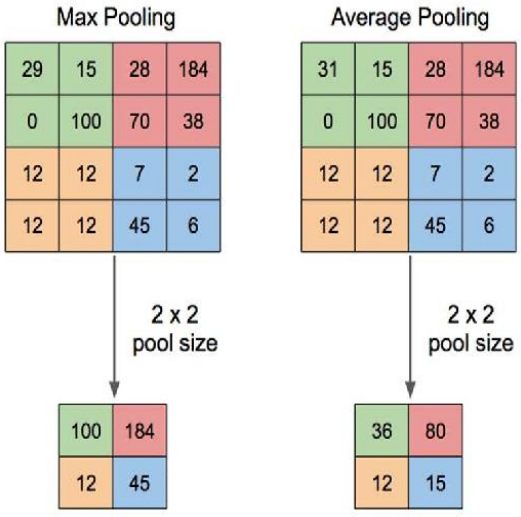

Figure 3.10 Max and average pooling operations [55]

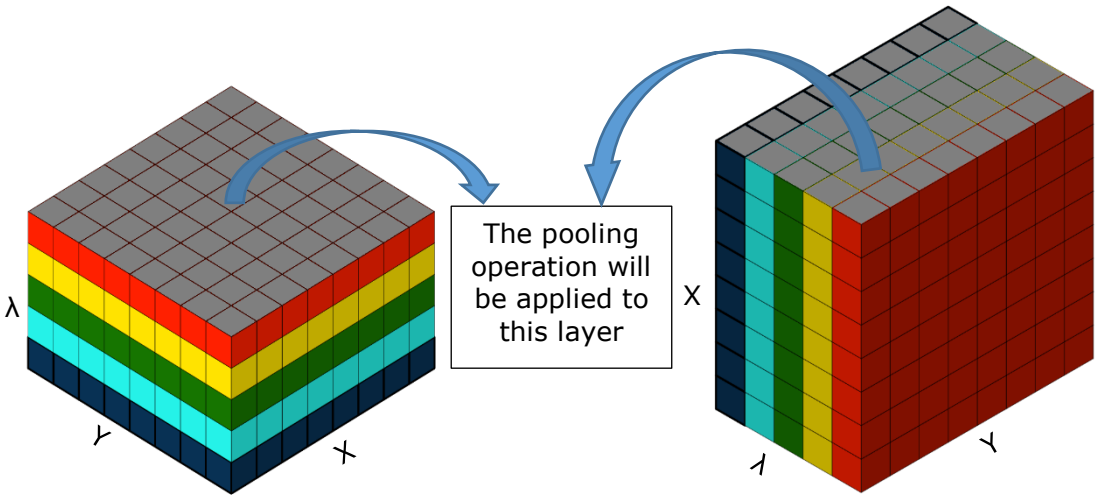

Figure 3.11 Pooling operation in general applications (left), in HSI (right)

After applying the pooling operation on the hyperspectral cube, the chosen wavelengths have been extracted and saved for classification on all pixels of data cube.

The author has been used the MATLAB code for maximum pooling operation on HSI, and selecting wavelengths (features), written by Dhanushka Chamara Liyanage, PhD student of Mechatronics and Autonomous Systems Centre of Tallinn University of Technology [56]. The 20 selected wavelengths using this code are presented in Table 3.3.

Table 3.3 Selected wavelengths using maximum pooling

Layer No.	Wavelength (nm)	Layer No.	Wavelength (nm)	Layer No.	Wavelength (nm)	Layer No.	Wavelength (nm)
9	420	57	560	106	705	151	841
19	449	65	583	116	735	161	871
29	478	74	610	122	753	171	902
40	510	83	637	132	783	181	932
50	539	95	672	142	813	191	963

3.5.2 Learning process of NN

After feature extraction, 500 pixels of each class have been selected as the references for learning. For finding the best NN classifier, different NN with different structures for both methods of feature extraction (local extremums and max-pooling operation) have

been tested. The structure of two of these NNs, which provided the most satisfactory results, have been presented in Table 3.4, and Figure 3.12.

Table 3.4 Structure of trained NNs

Model No.	**Activation functions of all hidden layers**	**Activation function of output layer**	**Training function**	**Performance function**	**Figure**
1	'tansig'	'softmax'	'trainscg'	'crossentropy'	Figure 3.12
2	'tansig'	'softmax'	'trainlm'	'mse'	

In Figure 3.12, the number of inputs is equal to 11 and 20 for local extremums and max-pooling operation as the band selection method, respectively.

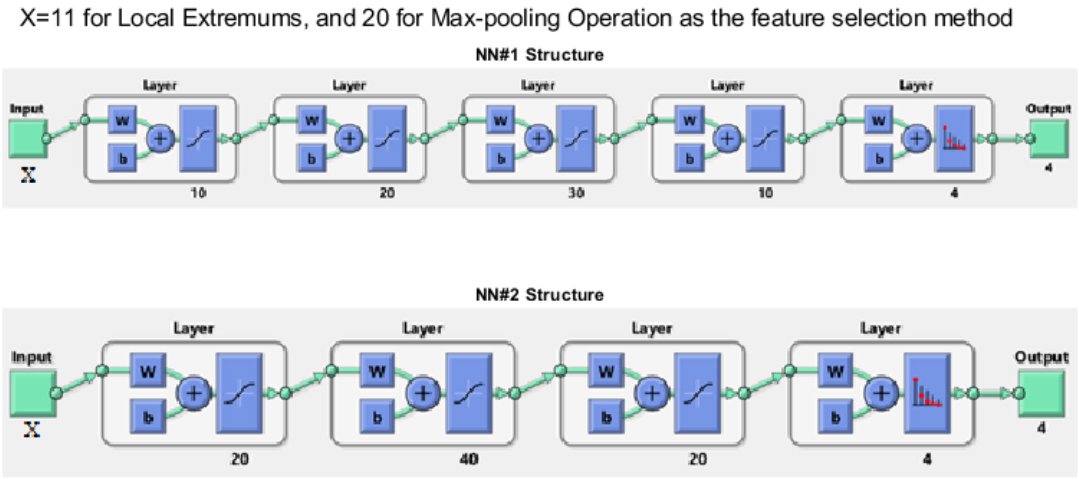

Figure 3.12 NNs structures

The training performances of these NNs with both methods of feature selection have been presented in Table 3.5. The numbers in Table 3.5 , shows the *crossentropy* and *mse* for NN#1 and NN#2, respectively.

Table 3.5 Training performances

	Local extremums as band selection method	Max-pooling operation as band selection method
NN#1 (crossentropy)	1,82e-12	4,58e-12
NN#2 (mse)	3,90e-16	5,92e-15

3.5.3 Testing process of NN

Figure 3.13 shows the results of two NNs classifiers with two methods of features selection (local extremums and max-pooling operation).

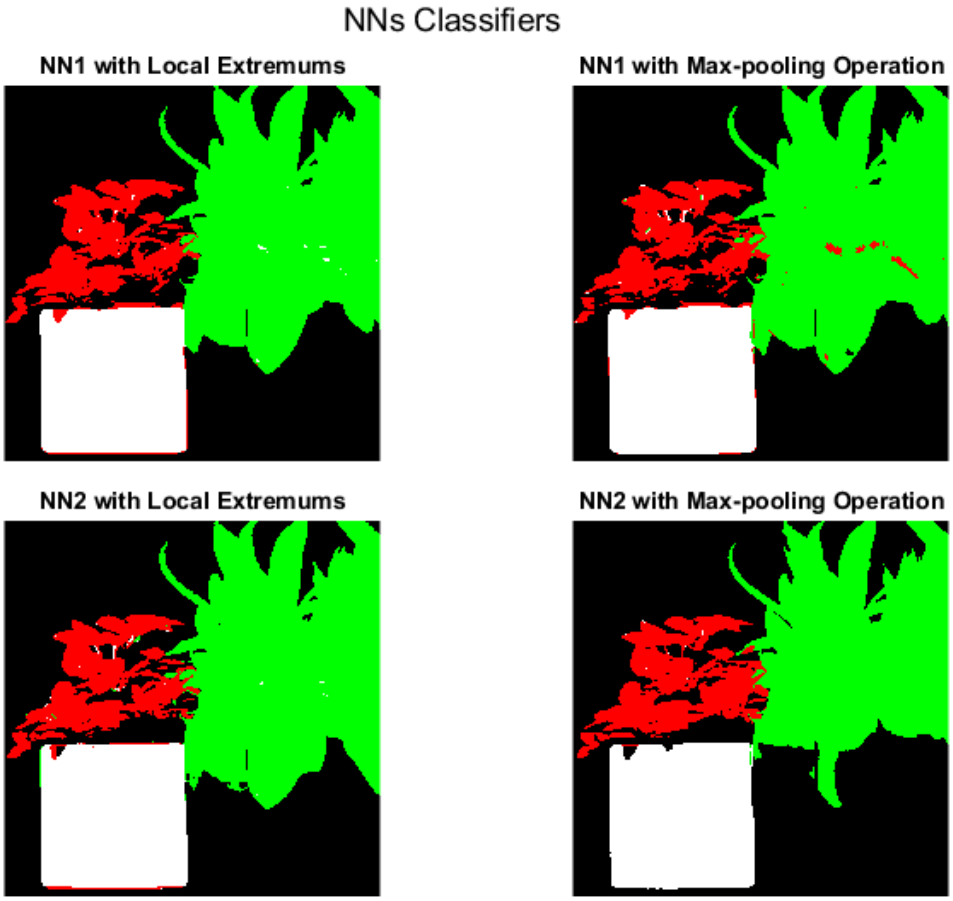

Figure 3.13 NNs classification results

To calculate the test performances of these classifiers, the original image has been masked manually. Then, the number of pixels which have been classified correctly, has been divided by the total number of pixels in the image (Equation 3.2). The final number shows the accuracy of classifier (Table 3.6).

Table 3.6 Test performances

	Local extremums as band selection method	Max-pooling operation as band selection method
NN#1 as the classifier	**81,40%**	75,31%
NN#2 as the classifier	76,84%	78,39%

3.6 Conclusion

In this chapter, firstly, spectral signatures of each pixel of the image have been extracted. Then, for preprocessing, using Savitzky-Golay filter, these spectral signatures have been smoothed for further processes. Secondly, the results of two models of classifiers, Spectral Angle Mapper (SAM) and Neural Network (NN), have been presented.

By comparing the test performance of SAM (57,81%), and test performances of two NN classifiers with two models of band selection (Table 3.6), it can be seen that the best test performance belongs to NN#1 (Figure 3.12), with local extremums as band selection model (81,40%). It means this classifier can correctly detect the material of more than 80% of pixels in the hyperspectral image.

On the other hand, the time taken for SAM to classify a hyperspectral image with dimensions of $512 \times 512 \times 204$ was less than two minutes; however, for NN classifiers, this time was more than five hours.

Hence, for applications in which being accurate is a more important concern than being fast, NN classifier is suggested as the principal solution, and on the contrary, when being fast is the issue of concern, SAM could be used as a solution.

4. OBJECT RECOGNITION

Despite the previous chapter that the hyperspectral data cube has been processed pixel-wise by the meaning of extracting and classifying spectral signature of each pixel separately, in this chapter, the hyperspectral data cube has been seen from a different angle. First, in this chapter, a workflow of solving this task using HSI has been presented. Then, the steps have been explained using practical experiments.

It is essential to know that this chapter tries to answer whether there is a relation between band selection and the result of object recognition or not. In other words, the focus of this chapter is to investigate whether or not there is a dependency between band selection for reconstructing a false RGB image, and the result of object recognition using pre-trained CNN.

4.1 Workflow

In object recognition task for a hyperspectral image, first, the idea of reconstructing a false RGB image from a hyperspectral data cube has been investigated. Then, it is tried to recognize the objects of the false RGB images using a pre-trained convolutional neural network (YOLO).

4.2 Image acquisition

For object recognition for hyperspectral images, the first step is to generate one dataset of images. For this purpose, the author has taken more than a hundred images from Tallinn University of Technology campus. This work has been done using SPECIM IQ hyperspectral mobile camera. Also, it was tried to take the images on sunny days, that means the presence of the sun as a suitable illumination source during image acquisition.

4.3 Reconstructing a false RGB image from an HSI

There are two main differences between an RGB image and an HSI, which should be considered when it is tried to extract an RGB from an HSI.

First, despite RGB camera which takes the image in three channels (red, green and blue), HSI takes the image in more than hundreds of bands, e.g. for SPECIM IQ hyperspectral mobile camera this number is equal to 204. The second difference is the range of the sensor for capturing the intensities. An RGB camera takes the image in

three channels, and the value of each pixel of a channel shows the integrated intensity over the wavelength range of the channel, between 0 to 255, although for HSI, this range might be quite different, e.g. for SPECIM IQ hyperspectral mobile camera this range is between 0 to 4096.

Therefore, it is needed first to extract three grayscale layers of an HSI, and then scale the intensities of the layer down from 0...4096 to 0...255.

4.3.1 Extracting three grayscale layers from an HSI

There are several ideas about how to extract three layers from a hyperspectral image for the creation of a false RGB image. One is to select the most critical three bands, and another is to combine several layers of HSI to achieve better false RGB image, which means the final false RGB image has the values of intensities more similar to a typical RGB camera.

To evaluate the first method, six different models of band selection were provided. The models and their reason for selection (description) have been presented in Table 4.1. The code has been written in MATLAB by the author to extract the selected layers, and save them for further processes.

Table 4.1 Band selection for a false RGB image extraction

Model Number	Layer Number	Wavelengths (nm)	Description
1	19	449	The layers suggested by SPECIM IQ Studio software [44]
	53	548	
	70	598	
2	26	470	The peaks of real RGB happened in these wavelengths [57]
	47	530	
	104	700	
3	9	420	The peaks of human cones graphs happened these wavelengths [58]
	47	530	
	57	560	
4	9	449	Three bands from the max-pooling operation 3.5.1)
	57	590	
	132	637	
5	6	410	Three bands selected at the very beginning of the spectral range of the camera
	9	420	

	12	430	
6	94	670	Three bands selected at the very end of the spectral range of the camera
	98	680	
	101	690	

4.3.2 Scaling the intensities

As it is mentioned, it is usually needed to scale the intensities of the selected layers down. Indeed, in HSI, with defining the white reference area in the image, it is possible to set the maximum of the intensity captured by the camera. Also, the minimum of the intensity comes from the dark reference, which means that no light should go through the lens. For this purpose, usually, the lens will be covered, and one image will be captured, however, in SPECIM IQ hyperspectral mobile camera, the dark reference has been predefined.

For scaling the intensities in this project, the relation between the intensities in RGB and HSI image has been assumed linearly. Therefore, the scaling can be done for each pixel separately using Equation 4.1, where I_{RGB} is the scaled pixel's intensity of one of the channels (red, green or blue), I_{HSI} is the pixel's intensity of the selected band of HSI, and I_{White} and I_{Dark} show the maximum and minimum pixel's intensities captured by hyperspectral camera, respectively.

$$I_{RGB} = 255 \times \left(\frac{I_{HSI} - I_{Dark}}{I_{White} - I_{Dark}} \right) \qquad \text{Equation 4.1}$$

The reconstructed false RGB images of a hyperspectral image as an example with the six different models of band selection (4.3.1) have been presented in Figure 4.1.

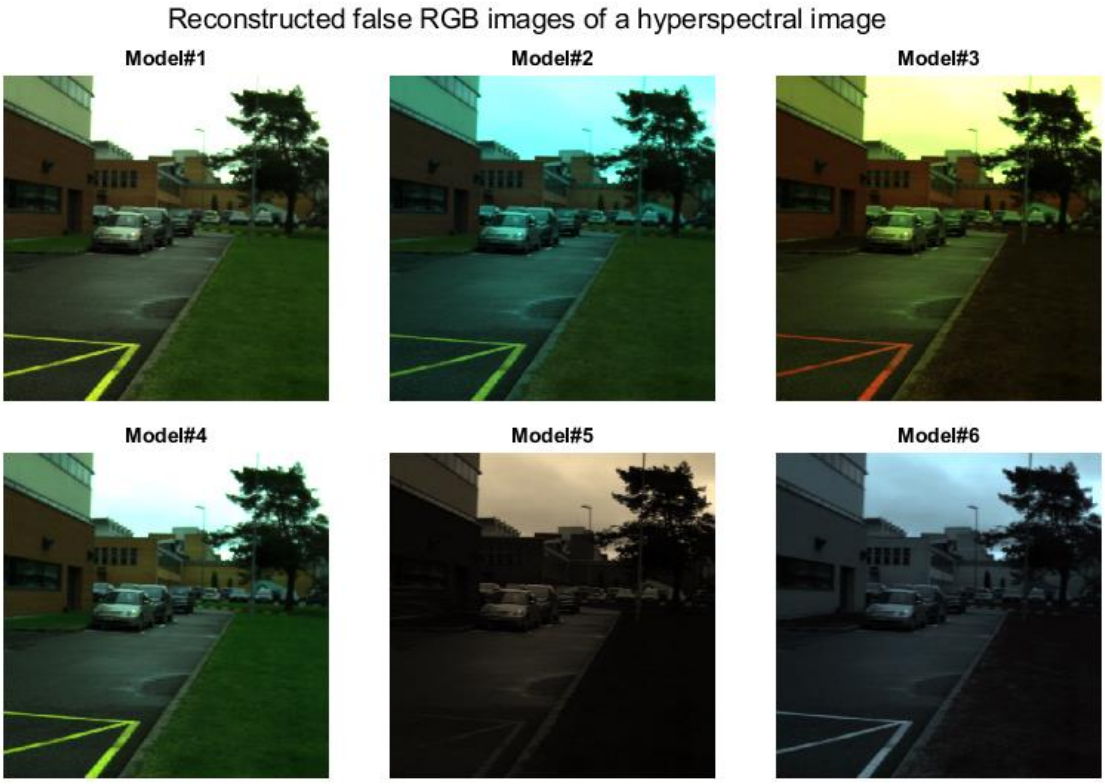

Figure 4.1 Reconstructed false RGB images of a hyperspectral image

4.4 Learning process of CNN

In this section, to evaluate the influence of band selection for reconstructing a false RGB image on the result of object recognition, a deep learning test has experimented.

For the implementation of any learning algorithm, the dataset generation is the first important step. Since one of the common objects among more than a hundred hyperspectral images of Tallinn University of Technology campus, which have been taken by the author, was cars, this object has been selected as the target of this learning.

In this work, a dataset of cars from back view with more than 300 images with 2D bounding box which shows the position of the car in the image has been used. To improve network accuracy, data augmentation has been done. Data augmentation randomly transforms the original data during training. In other words, with data augmentation, it is possible to add more variety to the training data without actually having to increase the number of labelled training samples [59], [60]. Some of the common techniques for image augmentations are rotating the image, flipping the image,

and adding noise to the image [61]. Augmented images of one of the images in the dataset have been shown in Figure 4.2.

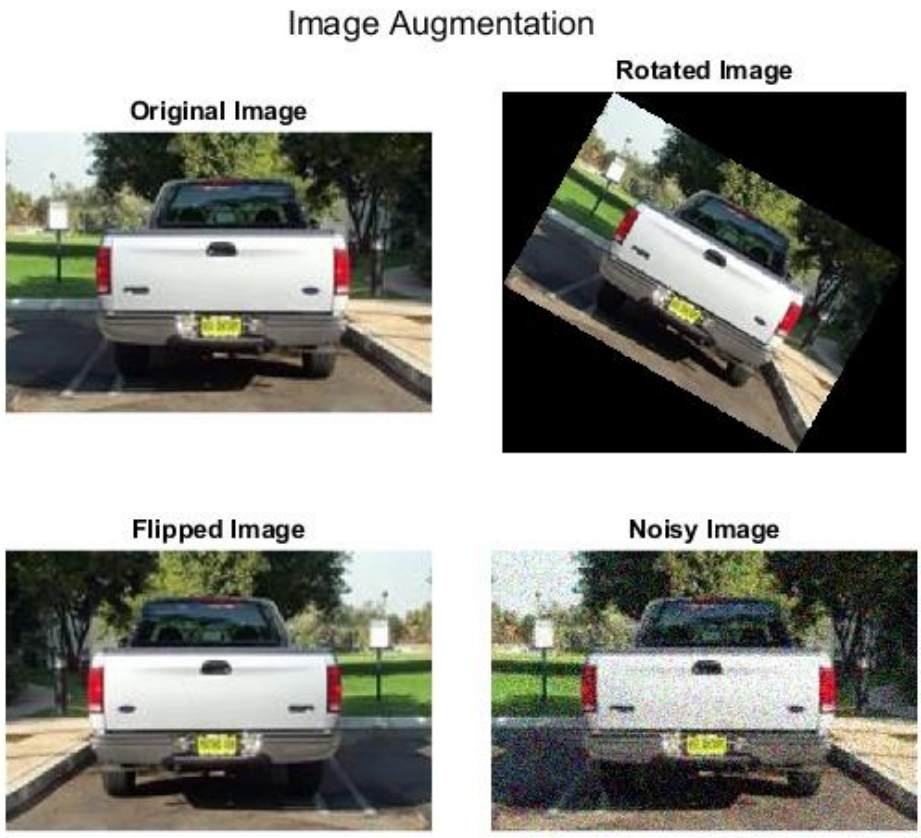

Figure 4.2 Image augmentation

After the dataset generation, YOLOv2 has been used for training the dataset [59].

4.5 Testing process of CNN

To find the influence of band selection models on the performance of object recognition, the false RGB images of all the hyperspectral images which had cars as an object inside the image, have been reconstructed. Then, they have been tested with the output of the trained neural network. Each image has been tested separately, and the objects in the image got a score which shows the similarity of the object found in the image with the car as the object. A score is a number between 0 and 1, and the higher number shows more similarity of the object and the car. The scores of three false RGB images with cars inside them have been shown as an example in Figure 4.3. The scores of these cars with different models of band selection (4.3.1) have been presented in Table 4.2.

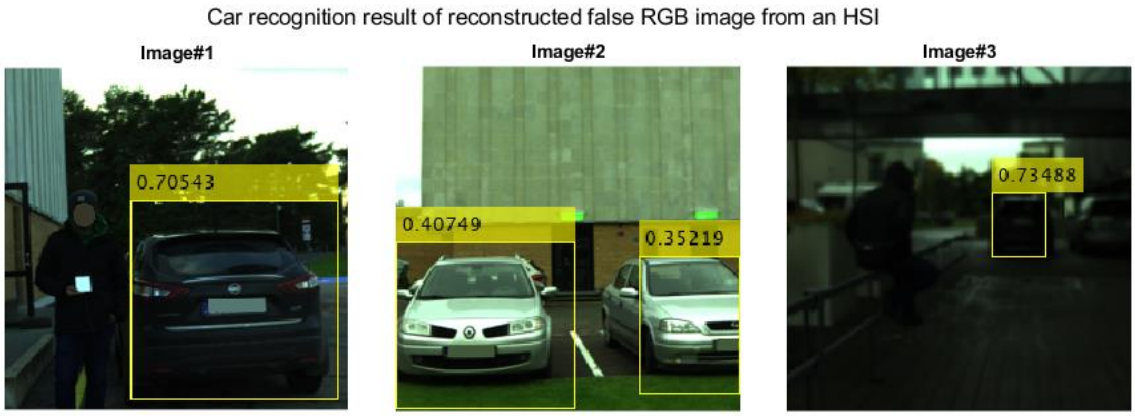

Figure 4.3 Car recognition result of reconstructed false RGB image from an HSI

Table 4.2 Car recognition result of reconstructed false RGB image from an HSI

Model of band selection	The score for the car in image#1	The score for the left car in image#2	The score for the car in Image#3
Model#1	0,70	0,40	0,73
Model#2	0,63	0,30	0,65
Model#3	0,65	0,34	**0,74**
Model#4	**0,75**	0,38	0,71
Model#5	0,67	**0,42**	0,71
Model#6	0,55	0,35	0,67

4.6 Conclusion

In this chapter, firstly, the way to reconstruct a false RGB image from an HSI has been explained. Then, to have different models of false RGB images, six models of layer selection have been presented. Finally, the results of object recognition task of YOLO for these models have been compared together.

By looking at the scores in Table 4.2, it can be interpreted that the result of object recognition of YOLO was not significantly depended on which model is used for the band selection. In other words, it seems that the selection of the three layers of an HSI for reconstructing a false RGB image for object recognition can be arbitrarily conducted and a great deal of consideration may not be needed.

SUMMARY

In this work, firstly, the influence of illumination sources on hyperspectral image acquisition results was studied, and the incandescent light and sun were proposed as the best illumination sources for indoor and outdoor hyperspectral imaging applications, respectively. Also, the spectral signatures of Aluminium Oxide (Al2O3), Aluminium Oxide plus Cubic Boron Nitride (cBN), and Wood by using two hyperspectral cameras, Resonon Pika II and Resonon Near Infrared, in the range of 400nm-1700nm (VIS and NIR) were acquired.

Secondly, the workflow for material classification using hyperspectral imaging was presented. For material classification, first, the spectral signature of each pixel was extracted, and the required preprocessing method (Savitzky-Golay filter) was applied. Then, to reduce the dimension of the features, two band selection methods (local extremums and max-pooling operation) were applied to the hyperspectral image, and 11 and 20 bands out of 204 bands were selected, respective to the band selection method. Finally, the result of Spectral Angle Mapper (SAM) classifier was compared with two neural network classifiers. Conclusively, when accuracy is a more important concern than classification speed, the principal suggested solution to the problem is NN, and when the speed of classification is the issue of concern, SAM could be used as a solution.

Thirdly, the idea of object recognition using a reconstructed false RGB image from a hyperspectral image was investigated. For this purpose, first, six different models of band selection for reconstructing a false RGB image were proposed. Then, using YOLOv2, a pre-trained convolutional neural network (CNN) for object recognition, the false RGB images were tested. The results show that the output provided by the object recognition agent is independent of the selected combination of the three layers (model of band selection) for reconstructing a false RGB image, or the level of dependency is so low that could be neglected considering the purpose and scope of this research work.

LIST OF REFERENCES

[1] A. Zahavi, A. Palshin, D. C. Liyanage, and M. Tamre, "Influence of illumination sources on hyperspectral imaging," in *Proceedings of the 2019 20th International Conference on Research and Education in Mechatronics, REM 2019*, 2019.

[2] "Hyperspectral Imaging: Techniques for Spectral Detection and Classification - Chein-I Chang - Google Books." [Online]. Available: https://books.google.ee/books?hl=en&lr=&id=JhBbXwFaA6sC&oi=fnd&pg=PA1&dq=Hyperspectral+imaging:+techniques+for+spectral+detection+and+classification&ots=r2jLCZK-vW&sig=7yMUgOHTZ3qepCcwk7n5qFijB3s&redir_esc=y#v=onepage&q=Hyperspectral imaging%3A techniques for spectral detection and classification&f=false. [Accessed: 31-Dec-2019].

[3] "Techniques and Applications of Hyperspectral Image Analysis - Google Books." [Online]. Available: https://books.google.ee/books?hl=en&lr=&id=DqmWQk01mlIC&oi=fnd&pg=PR5&dq=Techniques+and+applications+of+hyperspectral+image+analysis",&ots=FBiMc7Omjp&sig=AsKFtDUqFtMlZNyxeI1GEjvGakA&redir_esc=y#v=onepage&q=Techniques and applications of hyperspectral image analysis"%2C&f=false. [Accessed: 31-Dec-2019].

[4] "What Is Deep Learning? | How It Works, Techniques & Applications - MATLAB & Simulink." [Online]. Available: https://www.mathworks.com/discovery/deep-learning.html. [Accessed: 31-Dec-2019].

[5] "Hyperspectral Imaging for Food Quality Analysis and Control - Google Books." [Online]. Available: https://books.google.ee/books?hl=en&lr=&id=FVTbineZq54C&oi=fnd&pg=PP1&dq=Hyperspectral+Imaging+for+Food+Quality+Analysis+and+Control&ots=HFOjRIPArM&sig=wiv-7Ol12Ykqg1lhXRHge9bVDmo&redir_esc=y#v=onepage&q=Hyperspectral Imaging for Food Quality Analysis and Control&f=false. [Accessed: 02-Jan-2020].

[6] "Reflection, Transmission, and Absorption." [Online]. Available: https://light-measurement.com/reflection-absorption/. [Accessed: 26-Nov-2019].

[7] "Absorption, reflection, and refraction of light | Maya | Autodesk Knowledge Network." [Online]. Available: https://knowledge.autodesk.com/support/maya/learn-explore/caas/CloudHelp/cloudhelp/2015/ENU/Maya/files/BoL-Absorption-reflection-and-refraction-of-light-htm.html. [Accessed: 26-Nov-2019].

[8] "Word of the week: Electromagnetic spectrum | Space | EarthSky." [Online]. Available: https://earthsky.org/space/what-is-the-electromagnetic-spectrum. [Accessed: 26-Nov-2019].

[9] "Electromagnetic Spectrum - Introduction." [Online]. Available: https://imagine.gsfc.nasa.gov/science/toolbox/emspectrum1.html. [Accessed: 26-Nov-2019].

[10] "Hyperspectral Image - an overview | ScienceDirect Topics." [Online]. Available: https://www.sciencedirect.com/topics/computer-science/hyperspectral-image. [Accessed: 02-Dec-2019].

[11] "Hyperspectral Imaging - an overview | ScienceDirect Topics." [Online]. Available: https://www.sciencedirect.com/topics/medicine-and-dentistry/hyperspectral-imaging. [Accessed: 02-Dec-2019].

[12] "The hyperspectral data cube is the result of a hyperspectral... | Download Scientific Diagram." [Online]. Available: https://www.researchgate.net/figure/The-hyperspectral-data-cube-is-the-result-of-a-hyperspectral-measurement-It-contains-for_fig1_241604678. [Accessed: 02-Dec-2019].

[13] P. Mishra, M. S. M. Asaari, A. Herrero-Langreo, S. Lohumi, B. Diezma, and P. Scheunders, "Close range hyperspectral imaging of plants: A review," *Biosystems Engineering*, vol. 164. Academic Press, pp. 49–67, 01-Dec-2017.

[14] Z. Xiong, D. W. Sun, X. A. Zeng, and A. Xie, "Recent developments of hyperspectral imaging systems and their applications in detecting quality attributes of red meats: A review," *Journal of Food Engineering*, vol. 132. pp. 1–13, Jul-2014.

[15] X. Li, R. Li, M. Wang, Y. Liu, B. Zhang, and J. Zhou, "Hyperspectral Imaging and Their Applications in the Nondestructive Quality Assessment of Fruits and Vegetables," in *Hyperspectral Imaging in Agriculture, Food and Environment*, InTech, 2018.

[16] J. E. Fowler, *COMPRESSIVE PUSHBROOM AND WHISKBROOM SENSING FOR HYPERSPECTRAL REMOTE-SENSING IMAGING*. .

[17] "Push Broom and Whisk Broom Sensors - L3Harris Geospatial." [Online]. Available: https://www.harrisgeospatial.com/Support/Self-Help-Tools/Help-Articles/Help-Articles-Detail/ArtMID/10220/ArticleID/16262/Push-Broom-and-Whisk-Broom-Sensors. [Accessed: 02-Dec-2019].

[18] "Write band-interleaved data to file - MATLAB multibandwrite." [Online]. Available: https://www.mathworks.com/help/matlab/ref/multibandwrite.html. [Accessed: 02-Dec-2019].

[19] "2.11 Pushbroom Scanner." [Online]. Available: http://wtlab.iis.u-tokyo.ac.jp/wataru/lecture/rsgis/rsnote/cp2/cp2-11.htm. [Accessed: 02-Dec-2019].

[20] "Three approaches to generate hyperspectral image: (a) whiskbroom... | Download Scientific Diagram." [Online]. Available: https://www.researchgate.net/figure/Three-approaches-to-generate-hyperspectral-image-a-whiskbroom-imaging-point_fig2_229555724. [Accessed: 03-Dec-2019].

[21] A. F. H. Goetz, "Three decades of hyperspectral remote sensing of the Earth: A personal view," *Remote Sens. Environ.*, vol. 113, no. SUPPL. 1, Sep. 2009.

[22] "Landsat 8 « Landsat Science." [Online]. Available: https://landsat.gsfc.nasa.gov/landsat-8/. [Accessed: 05-Dec-2019].

[23] "Landsat 8 Bands « Landsat Science." [Online]. Available: https://landsat.gsfc.nasa.gov/landsat-8/landsat-8-bands/. [Accessed: 05-Dec-2019].

[24] K. Jia, X. Wei, X. Gu, Y. Yao, X. Xie, and B. Li, "Land cover classification using Landsat 8 Operational Land Imager data in Beijing, China," *Geocarto Int.*, vol. 29, no. 8, pp. 941–951, Nov. 2014.

[25] T. Kuemmerle, V. C. Radeloff, K. Perzanowski, and P. Hostert, "Cross-border comparison of land cover and landscape pattern in Eastern Europe using a hybrid classification technique," *Remote Sens. Environ.*, vol. 103, no. 4, pp. 449–464, Aug. 2006.

[26] J. Delegido, L. Alonso, G. González, and J. Moreno, "Estimating chlorophyll

content of crops from hyperspectral data using a normalized area over reflectance curve (NAOC),” *Int. J. Appl. Earth Obs. Geoinf.*, vol. 12, no. 3, pp. 165–174, Jun. 2010.

[27] A. S. Nunez and M. J. Mendenhall, “Detection of human skin in near infrared hyperspectral imagery,” in *International Geoscience and Remote Sensing Symposium (IGARSS)*, 2008, vol. 2, no. 1.

[28] “A Gentle Introduction to Object Recognition With Deep Learning.” [Online]. Available: https://machinelearningmastery.com/object-recognition-with-deep-learning/. [Accessed: 30-Dec-2019].

[29] “Demystifying Object Detection and Instance Segmentation for Data Scientists.” [Online]. Available: https://towardsdatascience.com/a-hitchhikers-guide-to-object-detection-and-instance-segmentation-ac0146fe8e11. [Accessed: 02-Jan-2020].

[30] A. Andreopoulos and J. K. Tsotsos, “50 Years of object recognition: Directions forward,” *Comput. Vis. Image Underst.*, vol. 117, no. 8, pp. 827–891, 2013.

[31] Z.-Q. Zhao, P. Zheng, S.-T. Xu, and X. Wu, “Object Detection with Deep Learning: A Review.”

[32] P. Soviany and R. T. Ionescu, “Optimizing the Trade-off between Single-Stage and Two-Stage Deep Object Detectors using Image Difficulty Prediction.”

[33] “13.4. Anchor Boxes — Dive into Deep Learning 0.7.1 documentation.” [Online]. Available: https://d2l.ai/chapter_computer-vision/anchor.html. [Accessed: 02-Jan-2020].

[34] “Understanding Deep Learning for Object Detection – DEEP LEARNING VAULT.” [Online]. Available: http://zoey4ai.com/2018/05/12/deep-learning-object-detection/. [Accessed: 30-Dec-2019].

[35] J. Redmon, S. Divvala, R. Girshick, and A. Farhadi, “You Only Look Once: Unified, Real-Time Object Detection.”

[36] “Calculating the Emission Spectra from Common Light Sources | COMSOL Blog.” [Online]. Available: https://www.comsol.com/blogs/calculating-the-emission-spectra-from-common-light-sources/. [Accessed: 02-Dec-2019].

[37] “Aluminium oxide – Database of ATR-FT-IR spectra of various materials.”

[Online]. Available: http://lisa.chem.ut.ee/IR_spectra/paint/fillers/aluminium-oxide/. [Accessed: 02-Jan-2020].

[38] "near-infrared hyperspectral imaging camera | Laser 2000." [Online]. Available: https://www.laser2000.fr/en/hyperspectral-cameras/48082-hyperspectral-camera-pika-nir.html#download_anker_link. [Accessed: 02-Jan-2020].

[39] "Boron in Ceramics Industry." [Online]. Available: http://biotsavart.tripod.com/bci.htm. [Accessed: 02-Jan-2020].

[40] "Water absorption spectrum." [Online]. Available: http://www1.lsbu.ac.uk/water/water_vibrational_spectrum.html. [Accessed: 02-Jan-2020].

[41] H. Dong, T. Li, J. Leng, L. Kong, and G. Bai, "GCN: GPU-Based Cube CNN Framework for Hyperspectral Image Classification," in *Proceedings of the International Conference on Parallel Processing*, 2017, pp. 41–49.

[42] "Specim IQ - Hyperspectral Goes Mobile!" [Online]. Available: https://www.specim.fi/iq/. [Accessed: 02-Jan-2020].

[43] "Specim IQ Technical Specifications." [Online]. Available: https://www.specim.fi/iq/tech-specs/. [Accessed: 09-Dec-2019].

[44] "Specim IQ Studio - Software for the Specim IQ camera." [Online]. Available: https://www.specim.fi/iq/specim-iq-studio/. [Accessed: 09-Dec-2019].

[45] C. Ruffin and R. L. King, "The analysis of hyperspectral data using Savitzky-Golay filtering-theoretical basis. 1," 2003, pp. 756–758.

[46] "Department of Electrical Power Engineering and Mechatronics ESTIMATION OF MOISTURE CONTENT OF BIOFUEL PELLETS USING HYPERSPECTRAL DATA."

[47] S. Addamani, "Spectral Angle Mapper Algorithm for Remote Sensing Image Classification," 2014.

[48] "Spectral Angle Mapper." [Online]. Available: https://www.harrisgeospatial.com/docs/SpectralAngleMapper.html. [Accessed: 10-Dec-2019].

[49] "Applied Spectroscopy: A Compact Reference for Practitioners - Jerry Workman, Jr., Art Springsteen - Google Books." [Online]. Available:

https://books.google.ee/books?hl=en&lr=&id=OzAnX25h4soC&oi=fnd&pg=PP1&dq=+Applied+Spectroscopy:+A+Compact+Reference+for+Practitioners&ots=_oQCw3-6OR&sig=UIaBhnbWgs1l4-yWabGJJ9vEjyQ&redir_esc=y#v=onepage&q=SAM&f=false. [Accessed: 10-Dec-2019].

[50] "HyperSpectral Toolbox by davidkun." [Online]. Available: http://davidkun.github.io/HyperSpectralToolbox/. [Accessed: 13-Dec-2019].

[51] "Comprehensive Guide to 12 Dimensionality Reduction Techniques." [Online]. Available: https://www.analyticsvidhya.com/blog/2018/08/dimensionality-reduction-techniques-python/. [Accessed: 13-Dec-2019].

[52] M. A. Hall, "Correlation-based Feature Selection for Machine Learning," 1999.

[53] J. Masci, U. Meier, D. Ciresan, J. Schmidhuber, and G. Fricout, "Steel defect classification with Max-Pooling Convolutional Neural Networks," in *Proceedings of the International Joint Conference on Neural Networks*, 2012.

[54] "Max Pooling Definition | DeepAI." [Online]. Available: https://deepai.org/machine-learning-glossary-and-terms/max-pooling. [Accessed: 13-Dec-2019].

[55] "Illustration of Max Pooling and Average Pooling Figure 2 above shows an... | Download Scientific Diagram." [Online]. Available: https://www.researchgate.net/figure/Illustration-of-Max-Pooling-and-Average-Pooling-Figure-2-above-shows-an-example-of-max_fig2_333593451. [Accessed: 13-Dec-2019].

[56] D. C. Liyanage, R. Hudjakov, and M. Tamre, "Hyperspectral Image Band Selection Using Pooling."

[57] "Wavelength and Color - Maple Programming Help." [Online]. Available: https://www.maplesoft.com/support/help/Maple/view.aspx?path=MathApps/WavelengthAndColor. [Accessed: 16-Dec-2019].

[58] "The Physics of Light and Color - Human Vision and Color Perception | Olympus Life Science." [Online]. Available: https://www.olympus-lifescience.com/en/microscope-resource/primer/lightandcolor/humanvisionintro/. [Accessed: 16-Dec-2019].

[59] "Object Detection Using YOLO v2 Deep Learning - MATLAB & Simulink."

[Online]. Available: https://www.mathworks.com/help/deeplearning/examples/object-detection-using-yolo-v2.html. [Accessed: 18-Dec-2019].

[60] "1000x Faster Data Augmentation – The Berkeley Artificial Intelligence Research Blog." [Online]. Available: https://bair.berkeley.edu/blog/2019/06/07/data_aug/. [Accessed: 18-Dec-2019].

[61] "Image Augmentation for Deep Learning using PyTorch." [Online]. Available: https://www.analyticsvidhya.com/blog/2019/12/image-augmentation-deep-learning-pytorch/. [Accessed: 18-Dec-2019].

[62] "What is Wavelength (Spectral) Range? - StellarNet, Inc." [Online]. Available: https://www.stellarnet.us/what-is-wavelength-spectral-range/. [Accessed: 26-Nov-2019].

[63] "What is spectral resolution, and when is it needed? - HORIBA." [Online]. Available: https://www.horiba.com/us/en/scientific/products/raman-spectroscopy/raman-academy/raman-faqs/what-is-spectral-resolution-and-when-is-it-needed/. [Accessed: 26-Nov-2019].

[64] N. K. Keppy and M. Allen, "Understanding Spectral Bandwidth and Resolution in the Regulated Laboratory."

[65] "Spectral signatures." [Online]. Available: https://www.slideshare.net/KunalRathod2/spectral-signature. [Accessed: 27-Nov-2019].

APPENDICES

Appendix 1

Terminologies of hyperspectral imaging:

Spectral range

The range of the electromagnetic spectrum can be captured by the hyperspectral imaging system is defined as the spectral range [62]. For example, some hyperspectral cameras capture the image in the range of 400-700 nm, which is the visible and very near-infrared range of the electromagnetic spectrum.

Spectral resolution

The spectral resolution is defined as the ability to resolve spectral features in the electromagnetic spectrum. In other words, spectral resolution is the absolute limit of the ability of a hyperspectral camera to separate two spectral features [63]. The spectral resolution is an essential parameter of experiments, because in case that is too low, it causes losing spectral information, and if it is too high, it may cause unnecessary longer measurement time.

Bandwidth

Bandwidth shows the spectral distance between two contiguous bands. In other words, bandwidth has been defined as Full Width at Half Maximum (FWHM) response to a spectral line of light with a Gaussian intensity distribution (Figure 0.1)[64]. Also, Bandwidth describes the narrowest spectral feature that a hyperspectral imaging system can resolve.

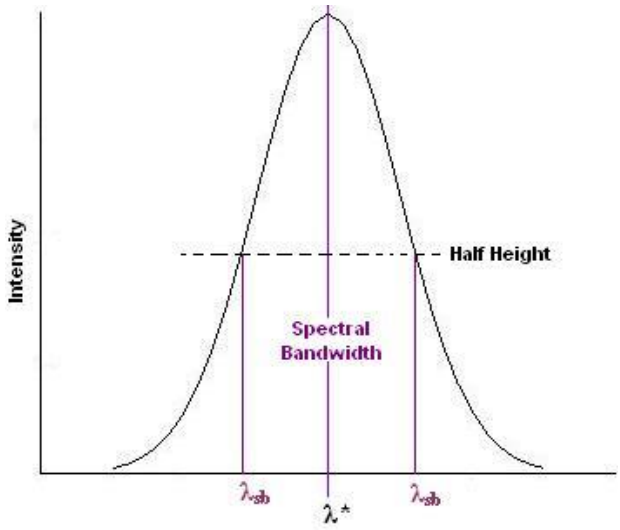

Figure 0.1 Bandwidth

Spectral signature

Depend on the wavelength, the sample will respond to the light emitted to it differently, and one of the goals in hyperspectral imaging is to plot this response characteristics of the material against wavelength. This plot has been defined as the spectral signature of the material [65]. For example, the spectral signature of green grass has been presented in Figure 0.2.

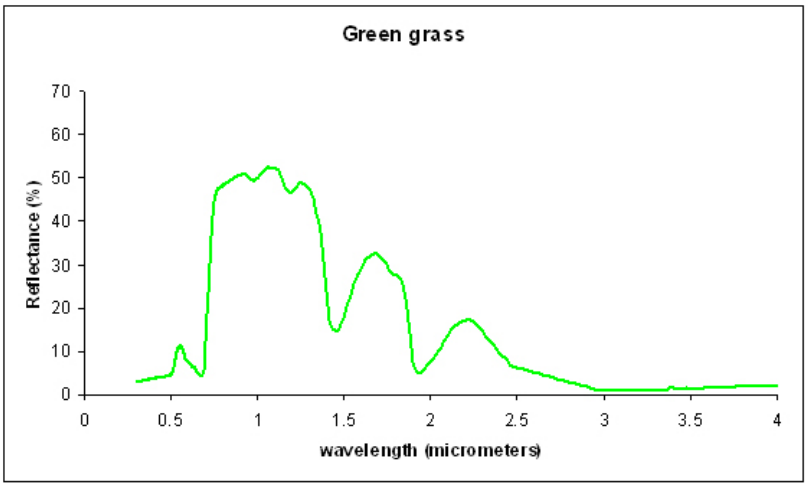

Figure 0.2 Spectral signature of green grass

Appendix 2

Table 0.1 The list of Landsat 8's bands and resolutions [27]

Band Number	Wavelength (μm)	Resolution (m)
1	0.433–0,453	30
2	0,450–0,515	30
3	0,525–0,600	30
4	0,630–0,680	30
5	0,845–0,885	30
6	1,560–1,660	30
7	2,100–2,300	30
8	0,500–0,680	15
9	1,360–1,390	30
10	10,6-11,2	100
11	11,5-12,5	100

Appendix 3

Table 0.2 The list of bands of SPECIM IQ camera [43]

Band No.	Wavelength (nm)	Band No.	Wavelength (nm)	Band No.	Wavelength (nm)	Band No.	Wavelength (nm)
1	397,32	52	545,62	103	696,61	154	850,29
2	400,20	53	548,55	104	699,60	155	853,33
3	403,09	54	551,49	105	702,58	156	856,37
4	405,97	55	554,43	106	705,57	157	859,42
5	408,85	56	557,36	107	708,57	158	862,46
6	411,74	57	560,30	108	711,56	159	865,50
7	414,63	58	563,24	109	714,55	160	868,55
8	417,52	59	566,18	110	717,54	161	871,60
9	420,40	60	569,12	111	720,54	162	874,64
10	423,29	61	572,07	112	723,53	163	877,69
11	426,19	62	575,01	113	726,53	164	880,74
12	429,08	63	577,96	114	729,53	165	883,79
13	431,97	64	580,90	115	732,53	166	886,84
14	434,87	65	583,85	116	735,53	167	889,90
15	437,76	66	586,80	117	738,53	168	892,95
16	440,66	67	589,75	118	741,53	169	896,01
17	443,56	68	592,70	119	744,53	170	899,06
18	446,45	69	595,65	120	747,54	171	902,12
19	449,35	70	598,60	121	750,54	172	905,18
20	452,25	71	601,55	122	753,55	173	908,24
21	455,16	72	604,51	123	756,56	174	911,30
22	458,06	73	607,46	124	759,56	175	914,36
23	460,96	74	610,42	125	762,57	176	917,42
24	463,87	75	613,38	126	765,58	177	920,48
25	466,77	76	616,34	127	768,60	178	923,55
26	469,68	77	619,30	128	771,61	179	926,61
27	472,59	78	622,26	129	774,62	180	929,68
28	475,50	79	625,22	130	777,64	181	932,74
29	478,41	80	628,18	131	780,65	182	935,81
30	481,32	81	631,15	132	783,67	183	938,88

31	484,23	82	634,11	133	786,68	184	941,95
32	487,14	83	637,08	134	789,70	185	945,02
33	490,06	84	640,04	135	792,72	186	948,10
34	492,97	85	643,01	136	795,74	187	951,17
35	495,89	86	645,98	137	798,77	188	954,24
36	498,80	87	648,95	138	801,79	189	957,32
37	501,72	88	651,92	139	804,81	190	960,40
38	504,64	89	654,89	140	807,84	191	963,47
39	507,56	90	657,87	141	810,86	192	966,55
40	510,48	91	660,84	142	813,89	193	969,63
41	513,40	92	663,81	143	816,92	194	972,71
42	516,33	93	666,79	144	819,95	195	975,79
43	519,25	94	669,77	145	822,98	196	978,88
44	522,18	95	672,75	146	826,01	197	981,96
45	525,10	96	675,73	147	829,04	198	985,05
46	528,03	97	678,71	148	832,07	199	988,13
47	530,96	98	681,69	149	835,11	200	991,22
48	533,89	99	684,67	150	838,14	201	994,31
49	536,82	100	687,65	151	841,18	202	997,40
50	539,75	101	690,64	152	844,22	203	1000,49
51	542,68	102	693,62	153	847,25	204	1003,58